AD-A036 212 M AND S COMPUTING INC HUNTSVILLE ALA F/G 17/9
PAR AURORAL STUDY. VOLUME VI. EFFECTS OF SIDELOBES ON THE OPERA--ETC(U)
DEC 76 P L ALLEY, J L BROWN, M J MITCHELL DASG60-74-C-0026
UNCLASSIFIED 76-0075 NL

1 OF 1
AD A036212

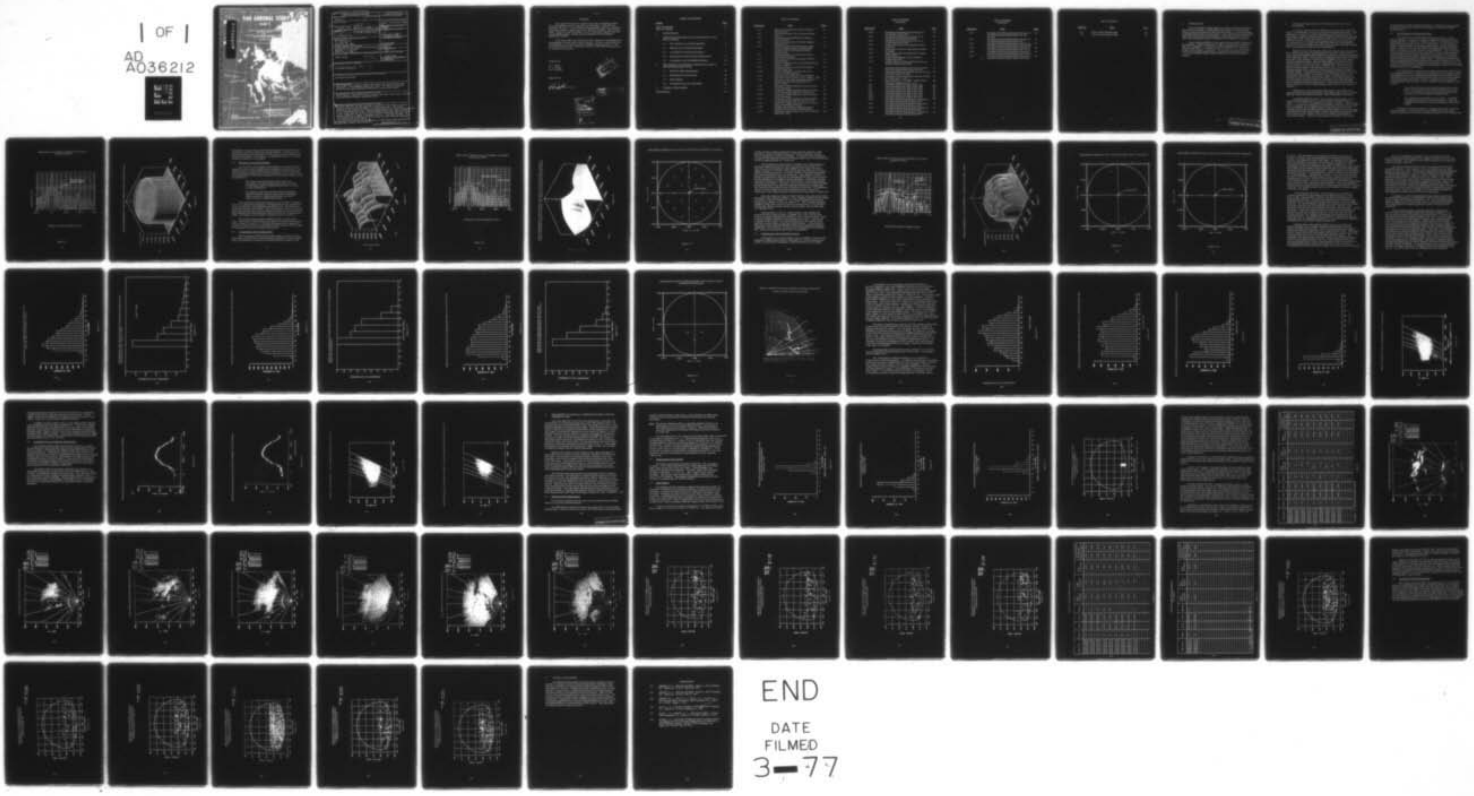

END

DATE FILMED
3-77

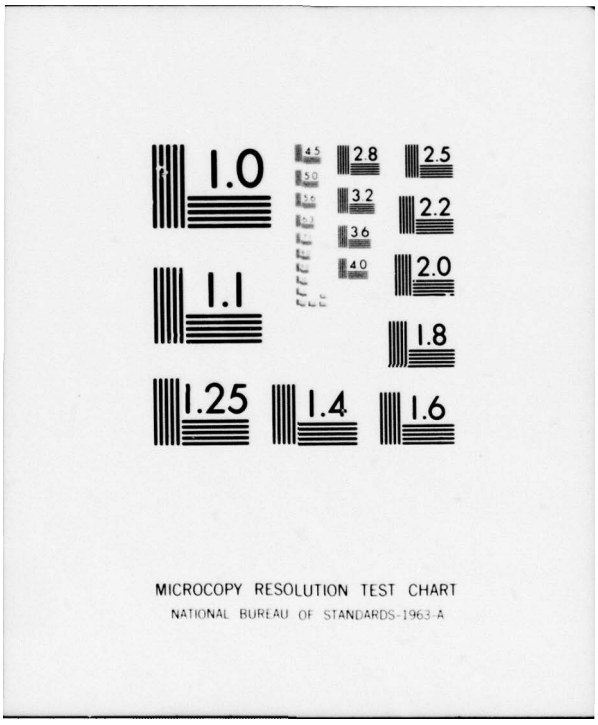
1.0
1.1
1.25
1.4
1.6
1.8
2.0
2.2
2.5
2.8
3.2
3.6
4.0
4.5
5.0
MICROCOPY RESOLUTION TEST CHART
NATIONAL BUREAU OF STANDARDS-1963-A

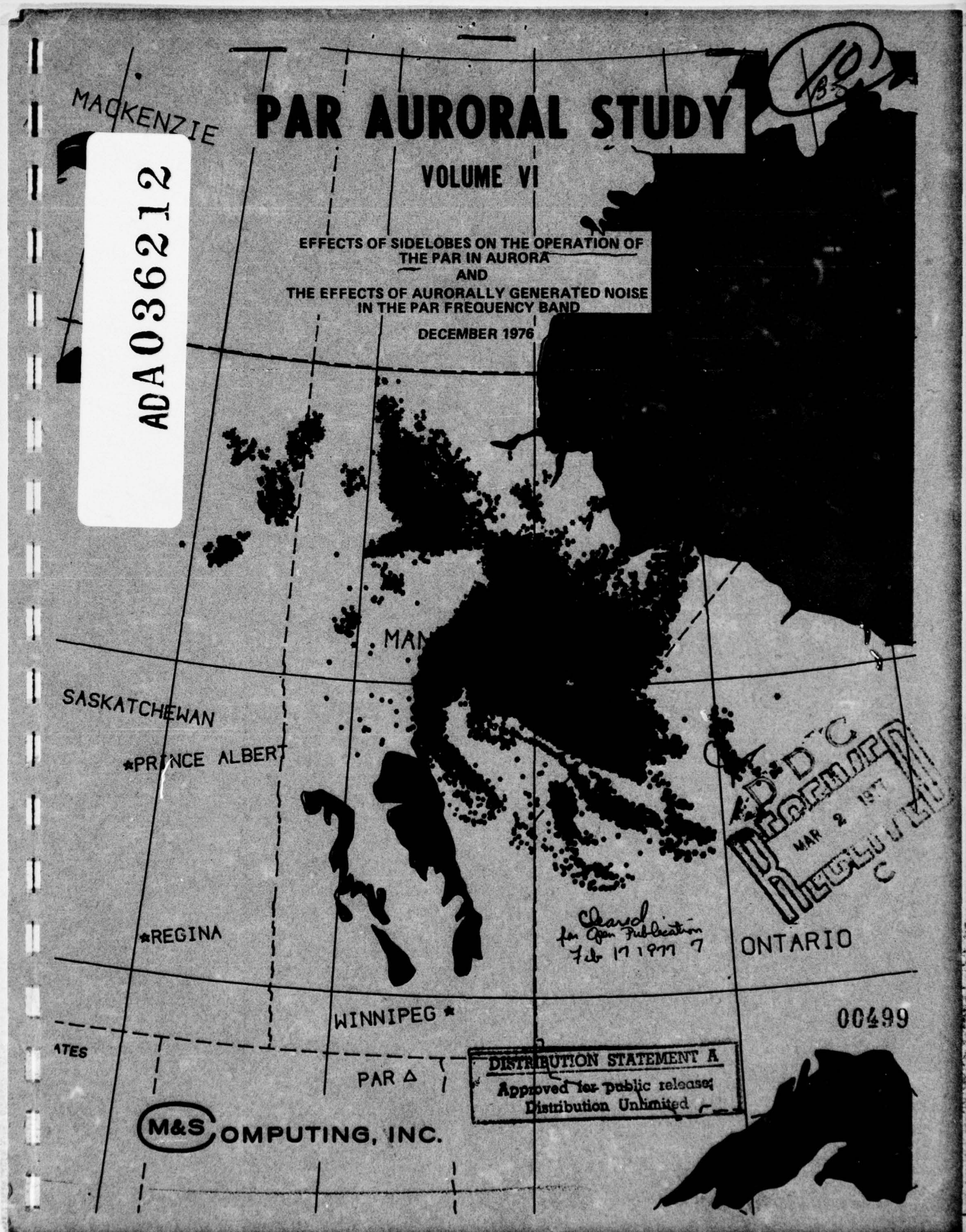

PAR AURORAL STUDY

VOLUME VI

EFFECTS OF SIDELOBES ON THE OPERATION OF THE PAR IN AURORA
AND
THE EFFECTS OF AURORALLY GENERATED NOISE IN THE PAR FREQUENCY BAND

DECEMBER 1976

M&S COMPUTING, INC.

SECURITY CLASSIFICATION OF THIS PAGE (When Data Entered)

REPORT DOCUMENTATION PAGE

READ INSTRUCTIONS BEFORE COMPLETING FORM

1. REPORT NUMBER: Volume VI
2. GOVT ACCESSION NO.
3. RECIPIENT'S CATALOG NUMBER

4. TITLE (and Subtitle): PAR Auroral Study. Operation of the Volume VI. Effects of Sidelobes on the PAR in Aurora and the Effects of Aurorally Generated Noise in the PAR Frequency Band.

5. TYPE OF REPORT & PERIOD COVERED: Interim - one of six volumes

6. PERFORMING ORG. REPORT NUMBER: 76-0075

7. AUTHOR(s): P. L. Alley, J. L. Brown, M. J. Mitchell et al

8. CONTRACT OR GRANT NUMBER(s): Army DASG60-74-C0026

9. PERFORMING ORGANIZATION NAME AND ADDRESS:
M&S Computing, Inc.
P. O. Box 5183
Huntsville, AL 35807

10. PROGRAM ELEMENT, PROJECT, TASK AREA & WORK UNIT NUMBERS: Not applicable

11. CONTROLLING OFFICE NAME AND ADDRESS:
US Army Ballistic Msl Defense Systems Command
BMDSC-WE, P. O. Box 1500
Huntsville, AL 35807

12. REPORT DATE: 10 Dec 76

13. NUMBER OF PAGES: 68

14. MONITORING AGENCY NAME & ADDRESS (if different from Controlling Office): Same as above. 75 p.

15. SECURITY CLASS. (of this report): Unclassified

15a. DECLASSIFICATION/DOWNGRADING SCHEDULE: Not applicable

16. DISTRIBUTION STATEMENT (of this Report):
Rept. no. 6 (Final),
Unlimited distribution

17. DISTRIBUTION STATEMENT (of the abstract entered in Block 20, if different from Report)
Unlimited distribution

18. SUPPLEMENTARY NOTES
This is one of six volumes of reports that present the aurora borealis data collected by a multi-megawatt phased array radar. The radar has excellent sensitivity and range resolution affording very precise aurora detail.

19. KEY WORDS (Continue on reverse side if necessary and identify by block number)
Aurora borealis, radar/aurora effects, phased array radar, aurora rads, satellite track perturbation effects, aspect sensitivity.

20. ABSTRACT (Continue on reverse side if necessary and identify by block number)
The report describes the data collected in connection with research of aurora borealis effects on the performance of a phased array radar. The primary objective of the study was to advance the understanding of the auroral phenomenon and of its interactions with radar. A multi-megawatt phased array radar was used to collect large quantities of high resolution auroral backscatter data with simultaneous tracking of a number of selected satellites. The report provides a detailed description of the data collection process and data reduction techniques in connection with auroral storms.

DD FORM 1 JAN 73 1473 EDITION OF 1 NOV 65 IS OBSOLETE

UNCLASSIFIED 406 226

SECURITY CLASSIFICATION OF THIS PAGE (When Data Entered)

1-A034 648
2 A034 503
3 A034 581
4-A034 504
5-A034 505

PREFACE

This report describes the results of two final investigations which were accomplished as part of the PAR Auroral Studies. This effort was performed for the U. S. Army Ballistic Missile Defense Systems Command in Huntsville, Alabama, under Contract No. DASG60-74-C0026. PAR Auroral Study, Volume VI, dated December 10, 1976, is the final volume is the PAR Aurora Studies series, and this volume constitutes M&S Computing's Report No. 76-0075.

Both of the study topics discussed in this volume are of significance to the designers of certain types of radar systems. The first subject deals with the potentially more serious problem of sidelobe blanking in aurora. The second describes a study to determine the level of PAR band noise generated in conjunction with aurora.

Prepared by:

P. L. Alley
J. L. Brown
M. J. Mitchell

Approved by:

W. E. Salter

W. E. Salter

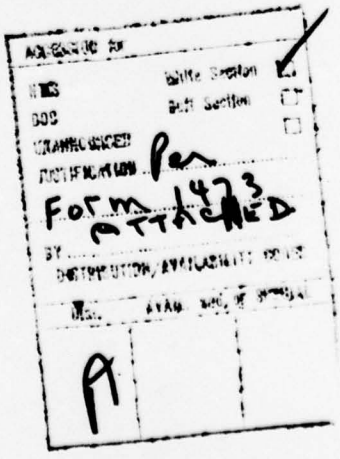

TABLE OF CONTENTS

LIST OF FIGURES

LIST OF FIGURES
(Continued)

LIST OF FIGURES
(Continued)

LIST OF TABLES

1. INTRODUCTION

This is the sixth and final volume in a series of reports describing the PAR Auroral Studies. The purpose of this study is to determine the effects of the aurora borealis on the operation of the U. S. Army Perimeter Acquisition Radar (PAR) in North Dakota. It is hoped that the results of this effort will be beneficial to the designers of future radar systems and that much of this information will be of interest to the scientific community.

Much of the background for this report was described in Volume I of the series [1]. Without reference to Volume I, portions of this discussion may seem ambiguous. It is therefore recommended that the reader be familiar with Volume I. Volumes II, III, IV, and V [2, 3, 4, and 5] also provide valuable supporting material. Each volume is available from the U. S. Army Ballistic Missile Defense Systems Command in Huntsville, Alabama.

2. EFFECTS OF SIDELOBES ON THE OPERATION OF THE PAR IN AURORA

It has been observed that the effective radar cross-section per unit volume, or reflectivity, of the aurora can reach relatively high levels. This reflectivity is, however, frequency dependent and is highest at the lower frequencies, dropping off from its peak only slightly in the 450 MHz operating region of the PAR. These high frequency levels, which have been observed to exceed 10^{-9} m^2/m^3, result in large effective radar cross-sections and very strong echoes, not only in the radar main beam but in the sidelobes. Auroral echoes in the sidelobes can easily be as strong as main beam echoes from normal targets ($<$20dB s/n) such as satellites.

Sidelobe echoes from the aurora affect the radar in two primary ways. First, these echoes may be superimposed on main beam echoes from the same range thus degrading the measurement of the true amplitude and position of the main beam target. This problem is especially severe when the auroral echo power in the sidelobe is of the order of magnitude of the echo power from the main beam target. This degrading effect was analyzed in more detail in Volume V of this series [5]. Unfortunately, there is no way of counteracting the effects of this type of sidelobe echo. The second major effect of auroral echoes in the sidelobes occurs when these echoes are detected independently of main beam returns and are treated as targets or potential targets. In the extreme case, it is possible that the auroral echoes could be detected, tracked, and mistaken for a threatening object. The probability of this situation is, however, slight. The biggest problem is that there may be so many of these echoes that the radar signal processor and controlling computer may become overloaded or seriously degraded by the excessive throughput requirements. A potentially serious problem is that the radar has no way of determining that these echoes come from the sidelobes.

Furthermore, when processing these returns, the location of the reflecting region is determined based on the pointing angle of the main beam. Sidelobe echoes will thus be mislocated, often by hundreds of kilometers.

Independent sidelobe echoes, such as those just described, can be controlled with various levels of success by using a sidelobe blanking system. For the PAR, this equipment is called a Q-channel. This Q-channel does a very good job of blanking unwanted sidelobe echoes from point targets such as satellites, but its effectiveness if reduced by the aurora, thus creating a worst-case operating situation for this equipment. It is the intent of this section to discuss the results of M&S Computing's investigation of the level of performance achieved by the PAR Q-channel during periods of auroral backscatter. Portions of the discussion presented in this section

are extracted from M&S Computing Report No. 75-0023 [6], which identified in detail the techniques employed in developing an improved Q-channel blanking pattern.

2.1 The Principal of Q-Channel Operation

It is an inherent characteristic of all practical radars to have antenna sidelobes or regions of secondary maxima at directions other than the primary lobe or main beam. Figure 2-1 shows a 0° aximuth cut of the PAR receive sum channel for the S1 or center beam. The Q-channel is simply a special antenna and receiving system which provides a reference pattern. This Q-channel antenna pattern is designed such that ideally its gain, at all angles, is greater than that of the sidelobes. Thus, if a target is at any angle other than that of the main beam, the echo power measured at the Q-channel will be greater than that from the main receive channel. The signal processing hardware employs this comparison on a continuous basis to eliminate independent sidelobe echoes. This ideal Q-channel would have an omnidirectional antenna pattern such as shown in Figure 2-1, and its receiver/signal processor would generate extremely low internal noise. The design of an omnidirectional Q-channel was undertaken; however, the resulting hardware did not prove satisfactory.

The original PAR Q-channel was a single element from the PAR array. In an ideal environment, a single element would have a power pattern closely approximating a cos θ curve (where θ is measured from the array normal). (See Figure 2-2 for a three-dimensional plot (in dB) of a cos θ power pattern.) In its actual setting at the PAR, however, the pattern for the Q-channel element showed erratic behavior and was deemed to be unacceptable for two reasons:

- The original Q-channel demonstrated relatively high noise levels. This is partially due to the extremely high amount of RF gain required to raise the Q-channel signal strength above the main receive beam first sidelobe level.
- The original Q-channel pattern was not ideal. It exhibited a considerable depression at lower elevations. This was attributed to the high level of ground reflections experienced at PAR.

Excellent documentary evidence, including actual radar Q-channel (element) patterns, was obtained during the PARPATS tests in which a beacon-carrying aircraft was used to generate signals as PAR-collected data.

MAIN ARRAY AND IDEAL Q-CHANNEL PATTERNS
(AZIMUTH CUTS)

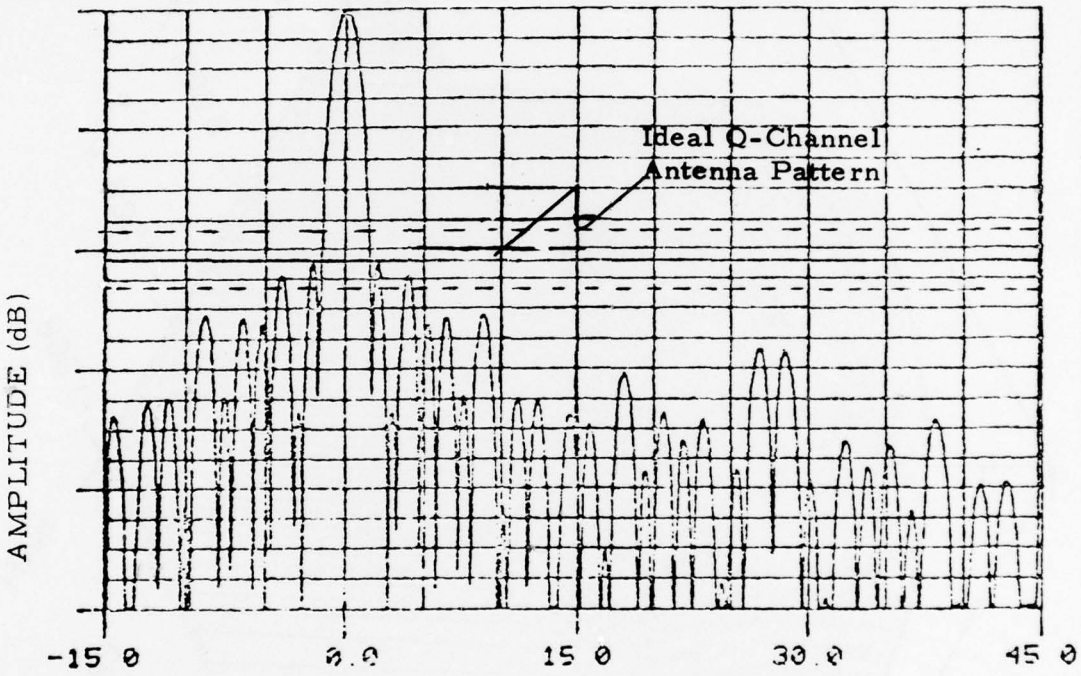

Figure 2-1

THREE-DIMENSIONAL VIEW OF ELEMENT POWER PATTERN (Cos θ)

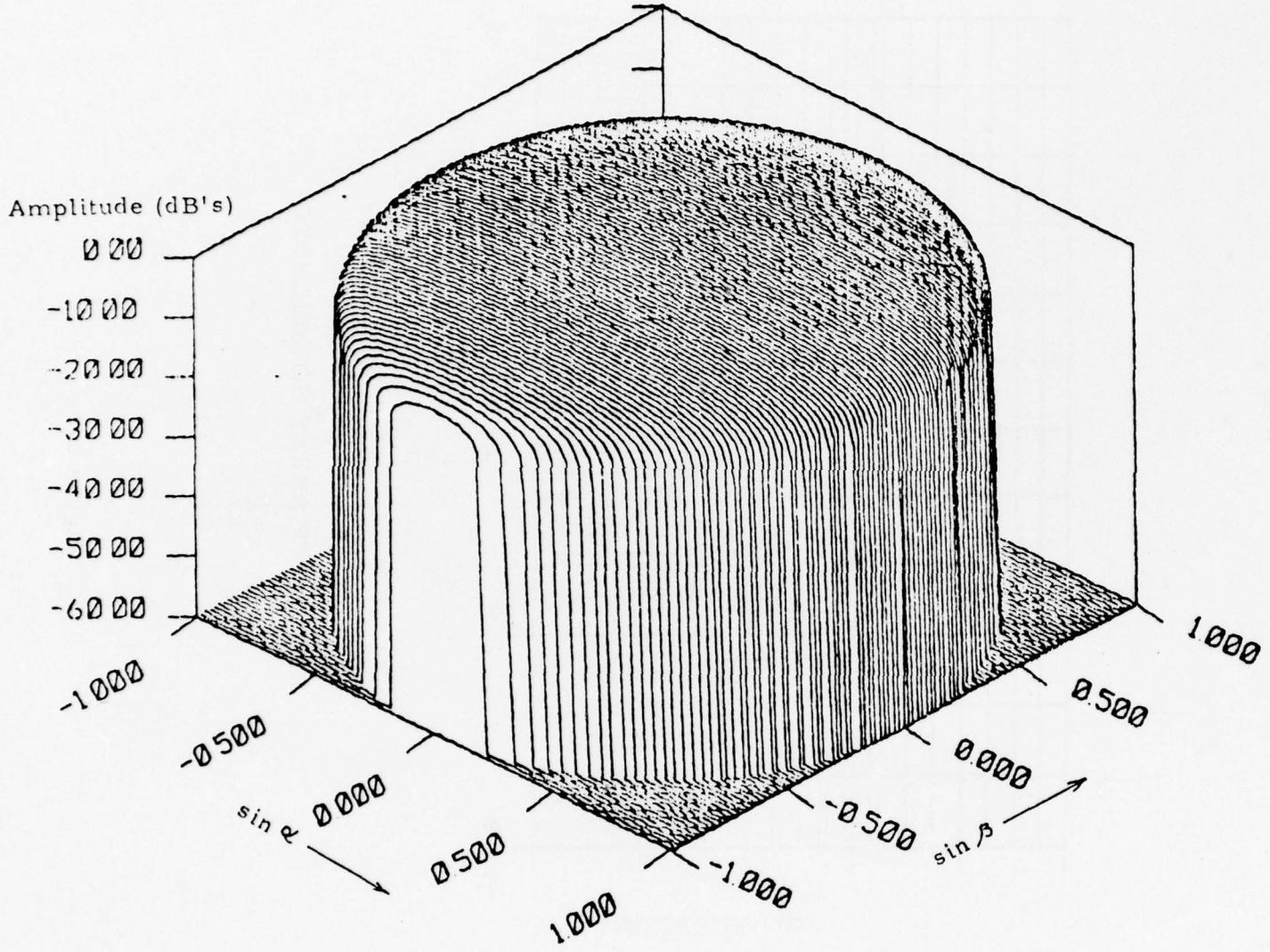

Figure 2-2

Fortunately, the previously mentioned element pattern distortion was not identical for each of the PAR array antenna elements. Furthermore, the tests showed that the irregularities over the entire array averaged out to produce an acceptable cosine pattern. Unfortunately, however, the single element Q-channel is not acceptable.

2.2 Subarray as a Q-Channel Antenna

As a solution to the problem, Bell Telephone Laboratories (BTL) suggested using a complete subarray of 24 elements as a Q-channel. The subarray could be steered with the main array and would always provide a smooth blanking threshold for the close-in sidelobes. This suggestion has been implemented at PAR, and has resulted in two immediate improvements in performance:

- The effects of ground reflections and certain other disturbances are reduced because the subarray pattern is directional, and the multiple elements tend to average out any irregularities.
- The signal-to-noise ratio at the Q-channel Comparator inputs is increased since the subarray has much higher antenna gain than a single element; thus, less downstream RF gain is required than before.

The subarray Q-channel does, however, have one major advantage. Since it is a multielement antenna, the Q-channel has its own arrangement of several sidelobes and associated nulls (Figure 2-3). No blanking can be provided at these null locations. Due to the geometry of the array, these nulls in the subarray pattern are located in the vicinity of several relatively high-amplitude main array sidelobes (referred to here as vestigial grating lobes). An example of this situation is shown in Figure 2-4 and 2-5.

The full PAR antenna pattern exhibits 22 such vestigial grating lobes. The location of each grating lobe relative to the main lobe at normal array is shown in Figure 2-6. This figure was generated by mapping the contours of regions which were not blanked by the Q-channel, thus revealing the main beam (center) and vestigial grating lobes.

2.3 A Proposed Q-Channel Improvement

M&S Computing recognized the possible impact of video detections, particularly auroral clutter, occurring in these unblanked vestigial grating lobes, and proceeded to develop a set of phase-tapering constants, used

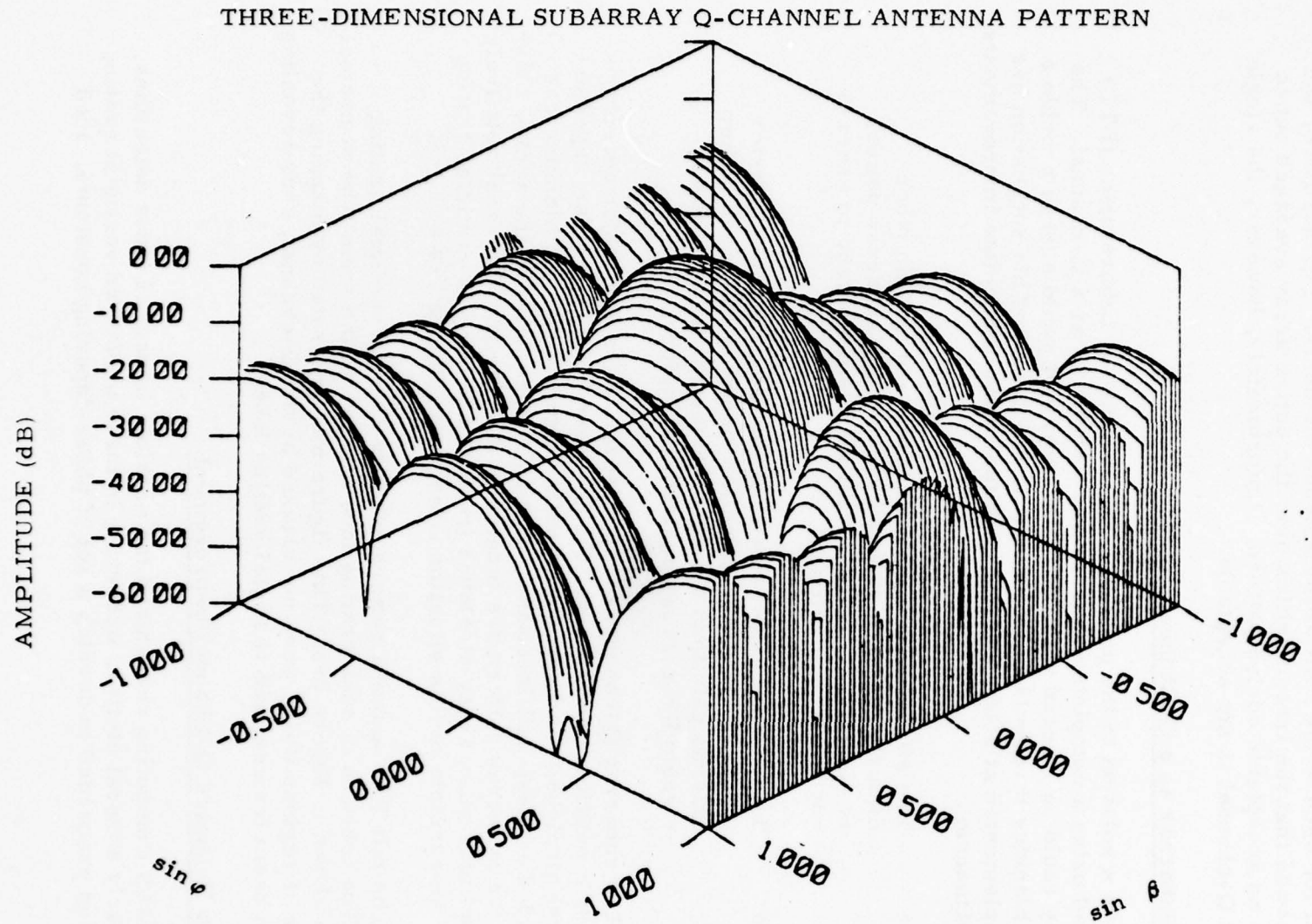
THREE-DIMENSIONAL SUBARRAY Q-CHANNEL ANTENNA PATTERN
AMPLITUDE (dB)
0 00
-10 00
-20 00
-30 00
-40 00
-50 00
-60 00
-1000
-0500
0000
0500
1000
sin φ
1000
0500
0000
-0500
-1000
sin β

Figure 2-3

MAIN ARRAY AND ACTUAL Q-CHANNEL PATTERNS
(AZIMUTH CUTS)

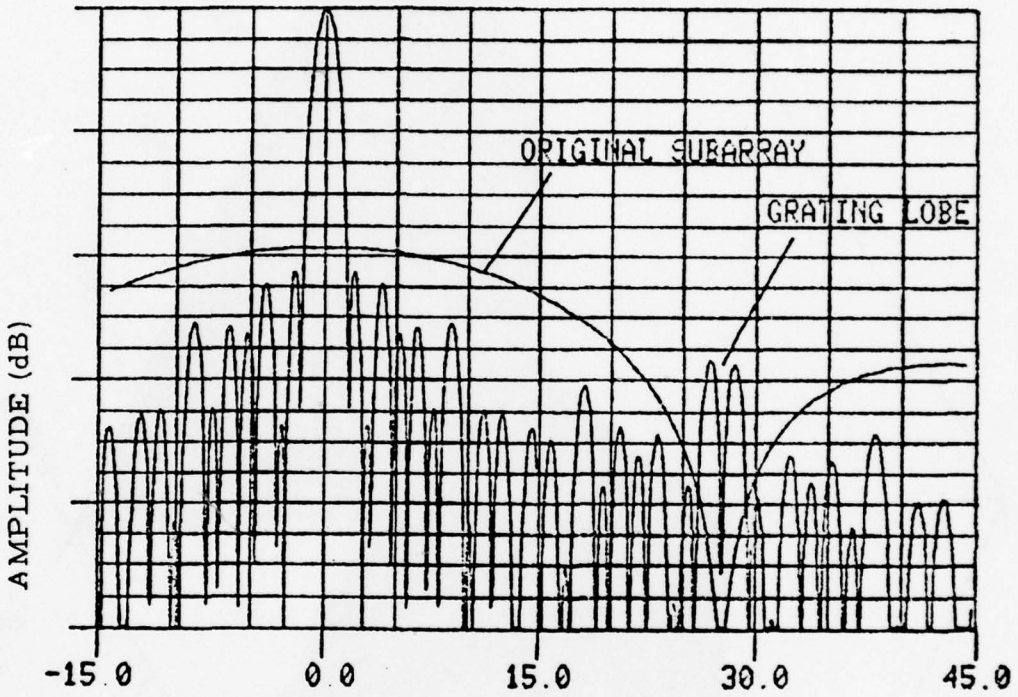

Figure 2-4

THREE-DIMENSIONAL PLOT SHOWING A DOUBLE PEAKED VESTIGIAL GRATING LOBE EXTENDING THROUGH A DIP IN THE BROAD Q-CHANNEL PATTERN BELOW

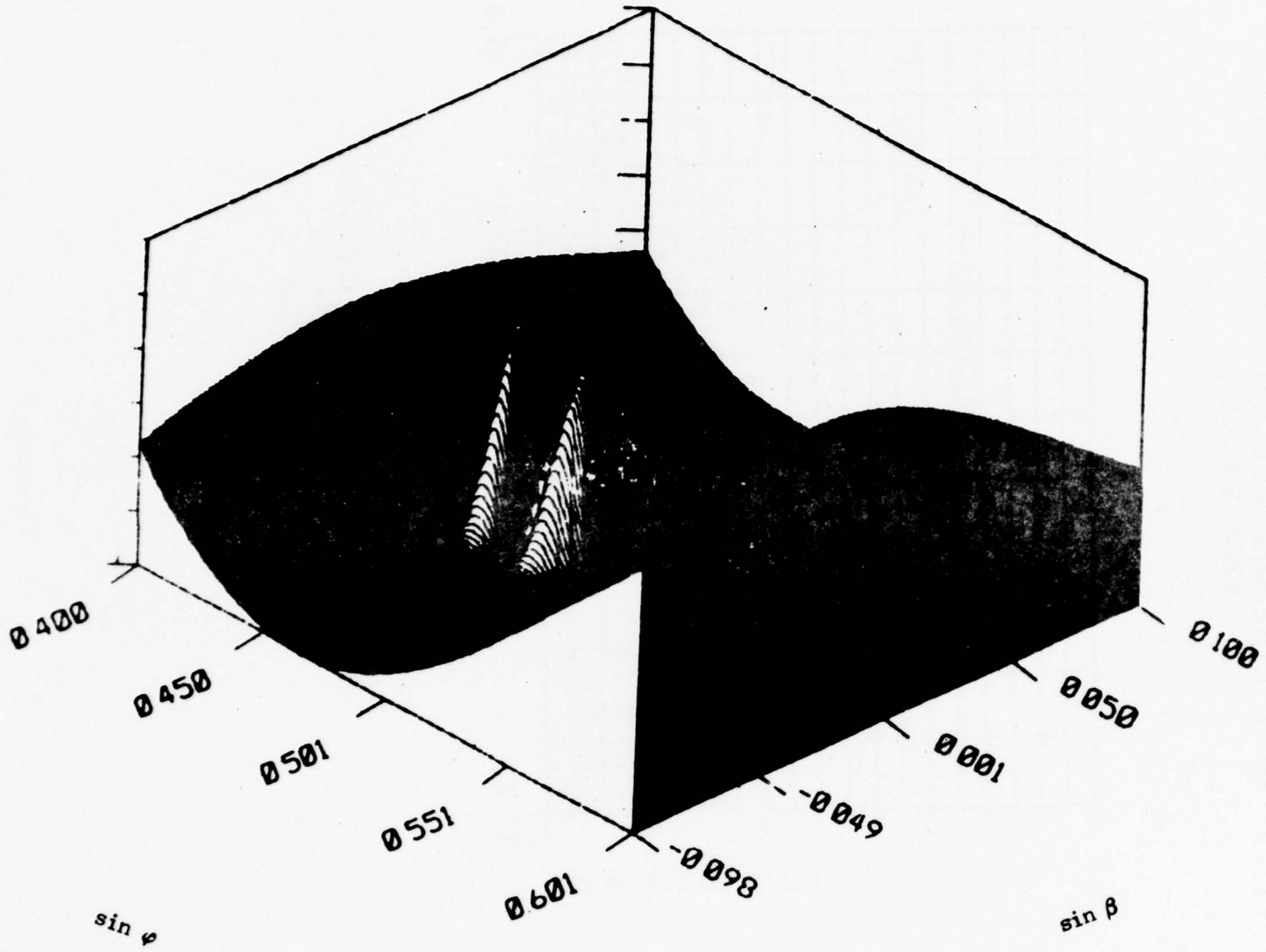

Figure 2-5

UNBLANKED REGIONS IN FULL PAR S1 PATTERN (UNMODIFIED SUBARRAY)

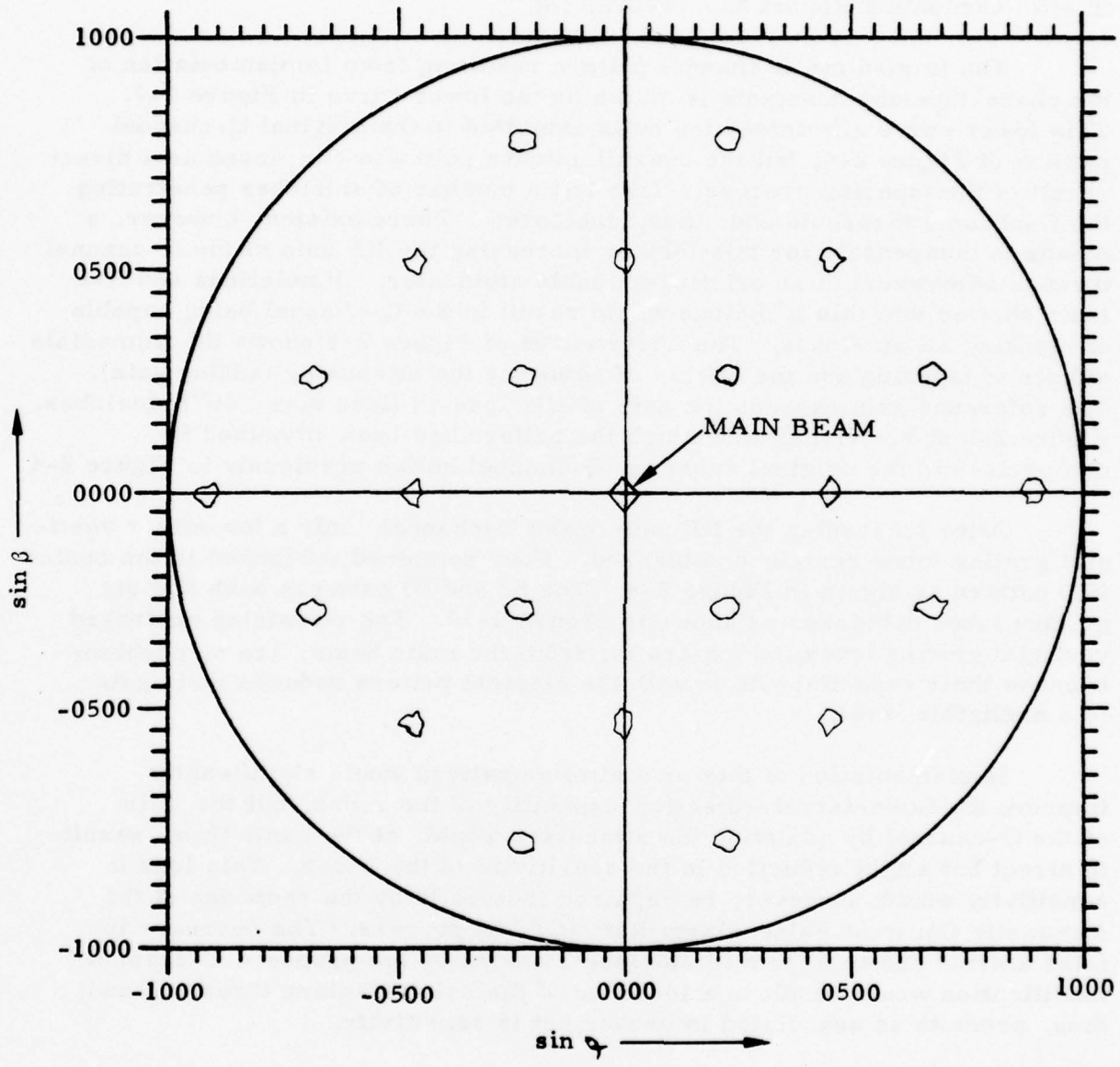

Figure 2-6

in beam steering, which would smooth out the subarray nulls and, at the same time, provide adequate blanking of the close-in sidelobes without serious degradation to receiver sensitivity. The details of the development process and the subsequent testing of the phase taper at the PAR are presented in M&S Computing Report No. 75-0023 [6].

The immediate Q-channel pattern resulting from implementation of the phase-tapering constants is shown as the lower curve in Figure 2-7. This lower curve eliminated the nulls exhibited in the original Q-channel pattern of Figure 2-4, but the overall antenna gain was decreased as a direct result of the tapering process. This left a number of sidelobes penetrating the Q-channel threshold and, thus, unblanked. There existed, however, a means to compensate for this loss by increasing the RF gain of the Q-channel through adjustment of an existing variable attenuator. Simulations and live tests showed that this technique would result in the Q-channel being capable of blanking all sidelobes. The upper curve of Figure 2-7 shows the immediate effects of tapering and the effects of adjusting the attenuator (adding gain). The reference gain exceeds the gain of all close-in (less than 45°) sidelobes. Figure 2-8 shows vividly how much the pattern has been smoothed in comparison to the original subarray Q-channel shown previously in Figure 2-4.

After increasing the RF gain of the Q-channel, only a few minor vestigial grating lobes remained unblanked. Four remained unblanked in the center (S1) pattern as shown in Figure 2-9. The S2 and S3 patterns each had six grating lobes unblanked as shown in Figure 2-10. The remaining unblanked vestigial grating lobes, which are far from the main beam, are no problem because their superimposition with the element pattern reduces their gain to a negligible level.

Implementation of this or a similar pattern would significantly improve the false-target-rejection capability of the radar, but the gain of the Q-channel by adjusting the attenuator would, at the same time, result in direct but slight reduction in the sensitivity of the radar. This loss in sensitivity would, however, be regained indirectly by the response of the Automatic Constant False Alarm Rate (CFAR) process. The decrease in false alarms due to improved sidelobe blanking by the proposed Q-channel modification would result in a lowering of the noise blanking threshold and, thus, promote as associated improvement in sensitivity.

2.4 Performance of the Q-Channel in Aurora

In the presence of normal targets, such as satellites, the gain of the unblanked vestigial grating lobes is sufficiently low, and the target size is usually so small that the probability of sidelobe detection of the targets

MAIN ARRAY AND ACTUAL Q-CHANNEL PATTERNS
(AZIMUTH CUTS)

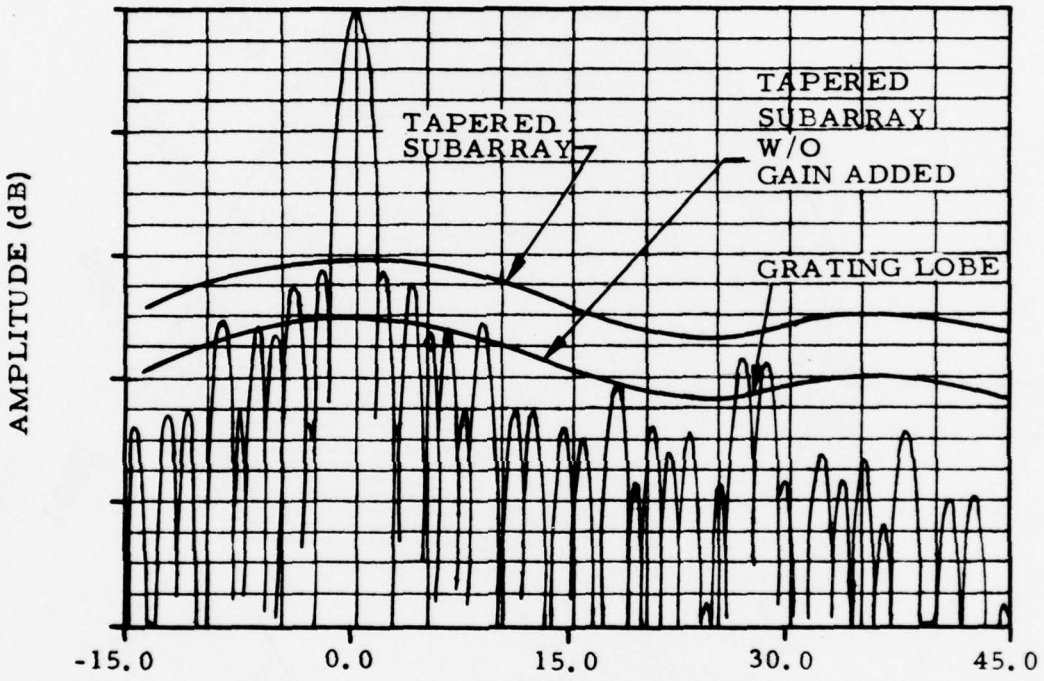

Figure 2-7

THREE-DIMENSIONAL VIEW OF MODIFIED SUBARRAY PATTERNS - X24Y27

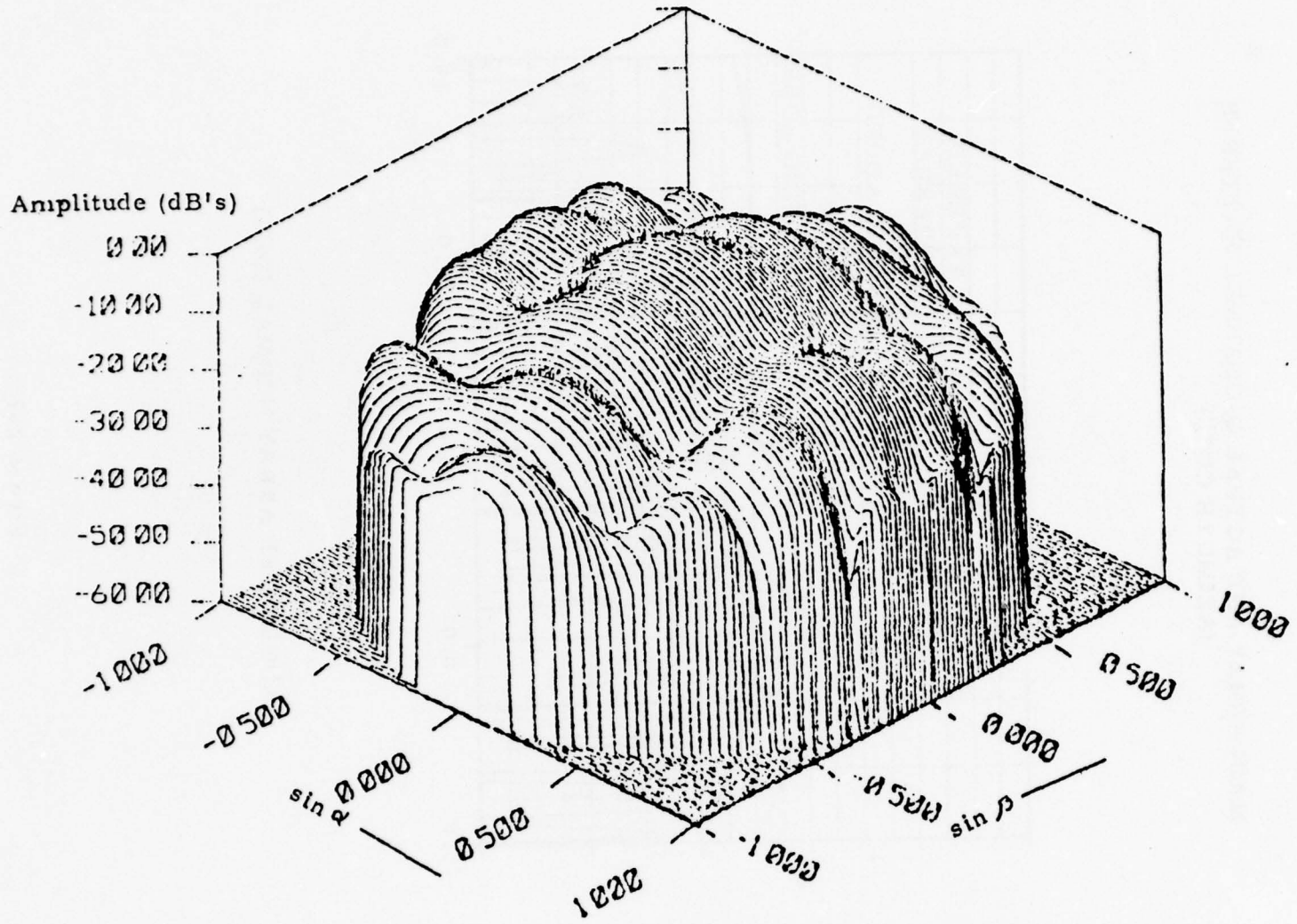

Figure 2-8

UNBLANKED REGIONS IN FULL PAR S1 PATTERN (X24Y27 SUBARRAY)

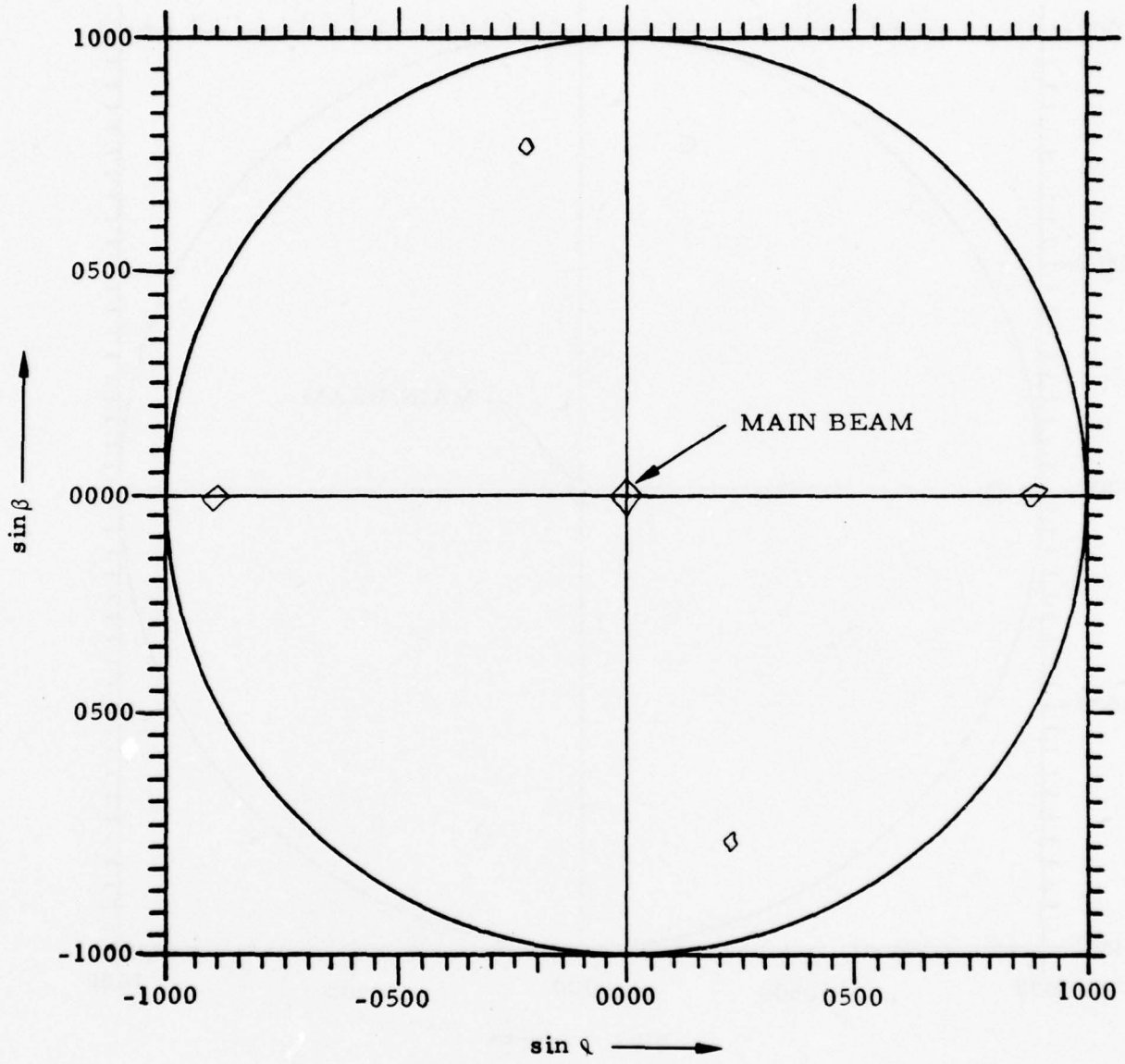

Figure 2-9

UNBLANKED REGIONS IN FULL PAR S2 OR S3 PATTERN (X24Y27 SUBARRAY)

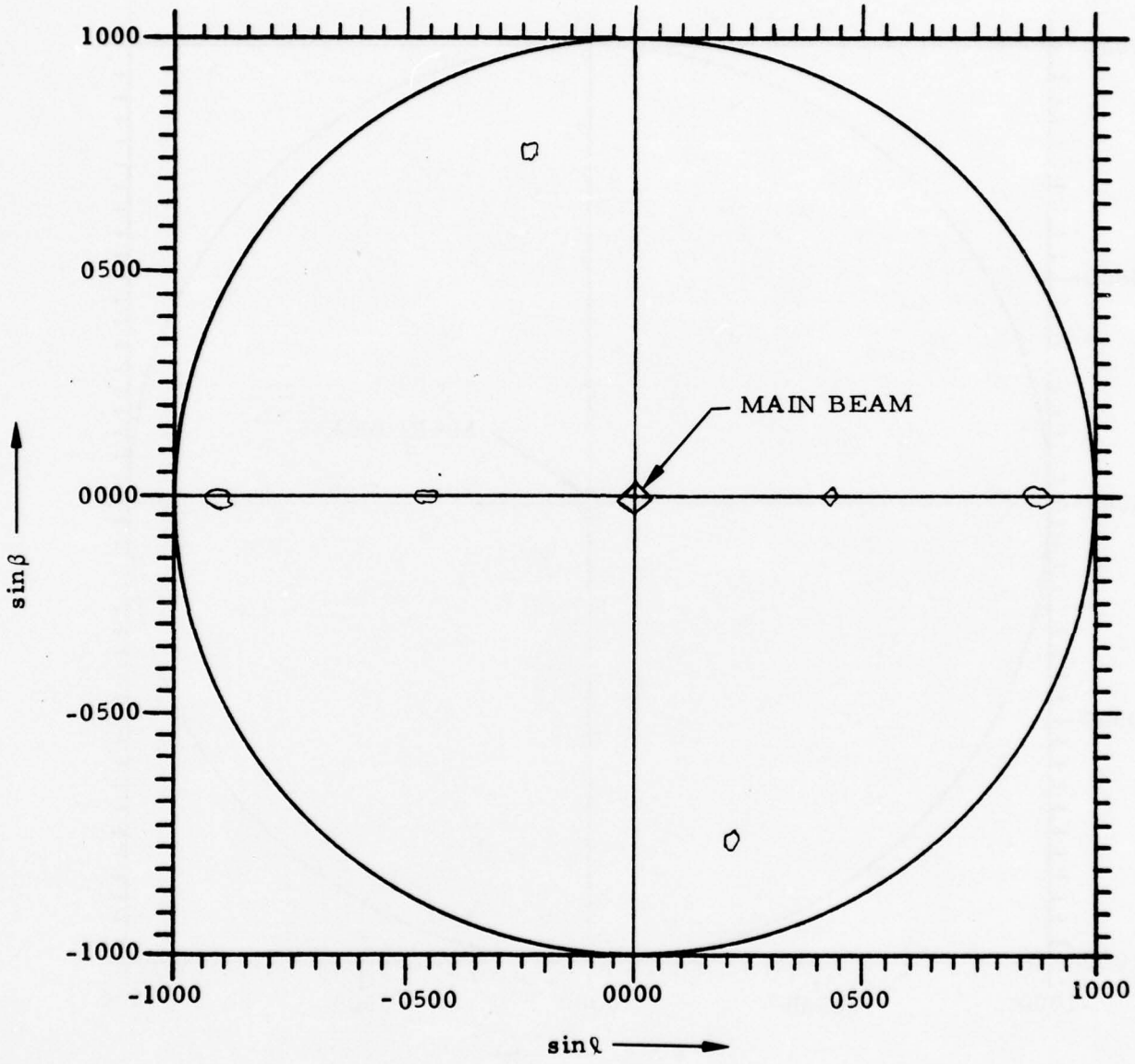

Figure 2-10

is remote. The tremendous cross-section presented by the aurora can, however, result in a great many detections in the unblanked sidelobes. In order to investigate the extent of this effect, an experiment was proposed which was intended to demonstrate the ability of the modified Q-channel to blank unwanted sidelobe returns from the vestigial grating lobes. This experiment consisted of periodically alternating, at frequent intervals, between the modified and unmodified Q-channel antenna patterns and then statistically comparing their performance differences. A simple technique was developed allowing this change to be made quickly by software control and by adjustment of a single attenuator. Unfortunately, however, on the only occasions when the auroral reflectivity was high enough to assure a valid test, the attenuator adjustment was not made, thus the Q-channel reference threshold was never raised as needed. The lower curve in Figure 2-7 shows the relationship of the Q-channel to the main beam antenna patterns. Thus, the experiment failed because at this gain level the close-in sidelobes penetrated the Q-channel threshold. This caused the performance of the modified Q-channel to appear worse than the original.

Even though this test failed, other techniques were available to evaluate certain performance features of the existing Q-channel. From these results, it was possible to surmise the effects of blanking by the proposed improvements. The technique employed in this analysis is practicable because the characteristics of the antenna patterns are known quite precisely. The key information available is the relative location and relative gain of the main beam and each vestigial grating lobe. During normal operation, the main beam is scanned over the entire reflecting region. During this period, some of the sidelobes will also be steered in the direction of the aurora, resulting in numerous returns. Due to the much lower gain of these sidelobes, the resulting echoes will be much smaller than the main beam echoes. By analyzing the distribution of reflectivities observed during any scan, it is possible to predict how may of these echoes might have originated from the unblanked vestigial grating lobes.

Previous study of the sidelobe levels present in the PAR power patterns indicated that the highest amplitude vestigial grating lobe was nearly 33 dB below the main lobe. The two-way transmit/receive pattern reduced this effective grating lobe level to approximately 66 dB. This means that the largest echoes from the vestigial grating lobes would be about 66 dB lower than main beam echoes from the same reflecting regions. The amplitude of any detected echo must also exceed a noise blanking threshold set at a level of approximately 10 dB s/n. Considering this threshold, it would be expected that in order to have detectable (10 dB s/n) echoes from the vestigial grating lobes, there would have to be regions of auroral reflectivity which would yield echoes of better than 76 dB s/n in the main beam.

From the distribution of detected echoes, the largest come from the main beam and only the smaller ones, usually less than 15 dB s/n, come from the sidelobes. Few sidelobe echoes would be expected if the maximum echoes were under 76 dB s/n.

The auroral backscatter data from the measurements made during the night of March 31, 1976, (April 1, 1976, u.t.) yielded raw s/n ratio peaks well in excess of the 76 dB minimum amplitude requirement established in the preceeding paragraph. In fact, return amplitudes of approximately 101 dB s/n were observed. Figure 2-11 shows a histogram of all returns detected during Scan 807 (10:24: 45-10:25: 13 u.t. April 1, 1976). The frequency of occurrence of the larger s/n detections is masked by the high frequency of occurrence of the smaller amplitude detections. Figure 2-12 is an expanded histogram of the high amplitude video detections with s/n ratios from 72-102 dB. Thirty dB of attenuation had been added to the signal processor front end to reduce the signal level below the signal processor saturation level. Figures 2-13 through 2-16 show additional samples of high amplitude detections with 12 dB front-end attenuation.

In Section 2.2, the 22 vestigial grating lobes which penetrated the Q-channel blanking pattern were described. Only the three grating lobes shown in Figure 2-17 need be of further concern. The remaining grating lobes are sufficiently far from the main lobe or oriented in such positions as to prevent them from being scanned into a region of strong auroral reflectivity.

At low elevations angles, when the main lobe is scanning the auroral volume, the vestigial grating lobes indicated in Figure 2-17 are steered into the ground or just below the auroral volume. However, as the main lobe is steered through elevations from $+3^{\circ}$ to $+16^{\circ}$ with respect to broadside (28° to 41° with respect to ground), these vestigial grating lobes are scanning the auroral volume. With intense auroral activity, as has already been shown significant sidelobe detections may be expected. Upon being processed and graphically displayed, these vestigial grating lobe returns will create a ghost image at the elevation where the appropriate sidelobes begin to scan the reflecting region. Main beam auroral echoes are limited by range-gate masking of all echoes from the auroral volume, but the ghost image just described extends outside of this volume so that these ghost echoes would not be eliminated. With a thin arc centered at an altitude of 105 km, the vestigial grating lobe echoes will be processed using the pointing angle of the main beam, resulting in an apparent (ghost) auroral band between 200 and 350 km altitude--well above the software auroral exclusion volume limitations. As shown in Figure 2-18, S_1 and S_2 refer to the lower and upper elevations for vestigial grating lobe illumination of the aurora. M_1 and M_2 refer to the corresponding main lobe positions.

HISTOGRAM OF ALL RETURNS DETECTED DURING SCAN 807
(10:24: 45-10:25: 13 U.T APRIL 1, 1976)

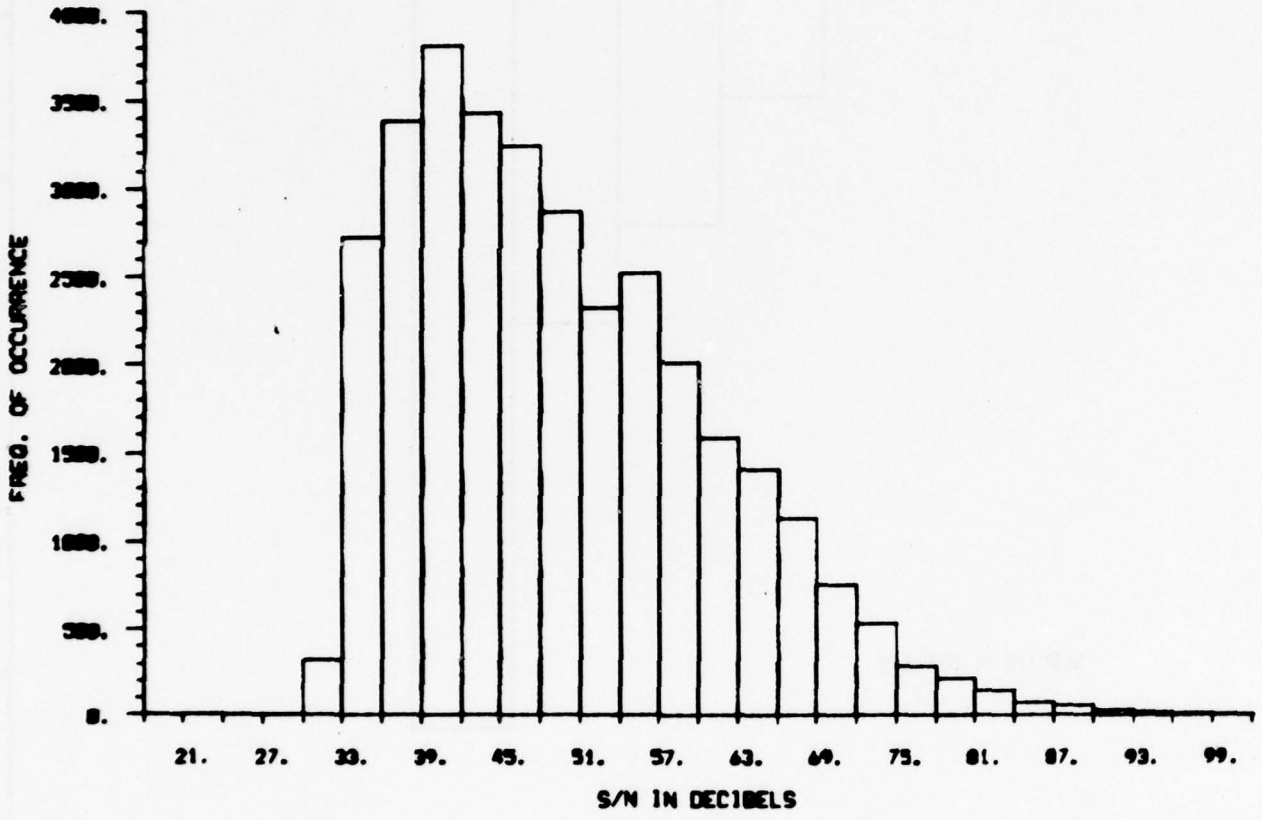

Figure 2-11

HISTOGRAM OF THE HIGH AMPLITUDE DETECTIONS DURING SCAN 807
(10:24:45-10:25:13 U.T. APRIL 1, 1976)

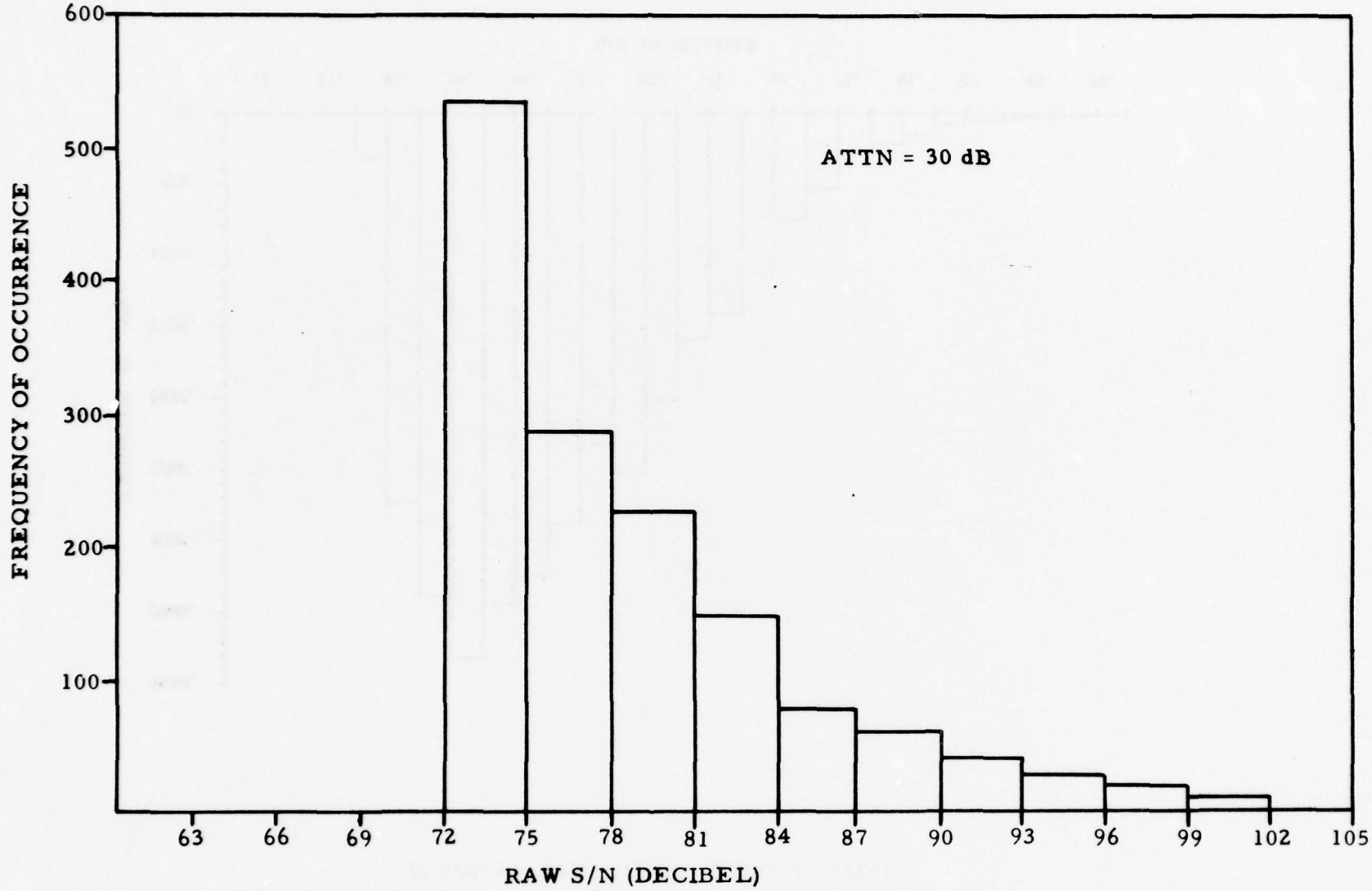

Figure 2-12

HISTOGRAM OF HIGH AMPLITUDE DETECTIONS WITH 12 DB ATTENUATION

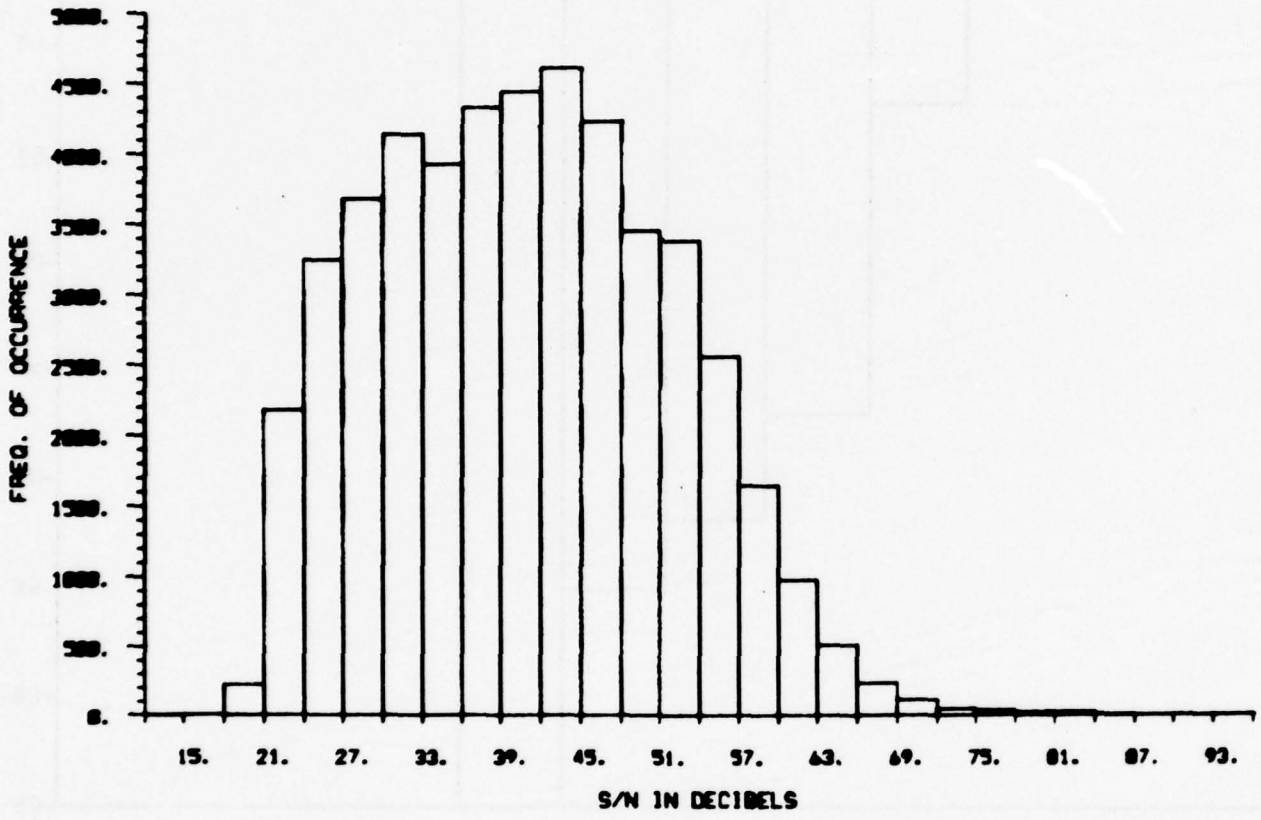

Figure 2-13

HISTOGRAM OF HIGH AMPLITUDE DETECTIONS WITH 12 dB ATTENUATION
(SCAN 743, 92/08/45/02)

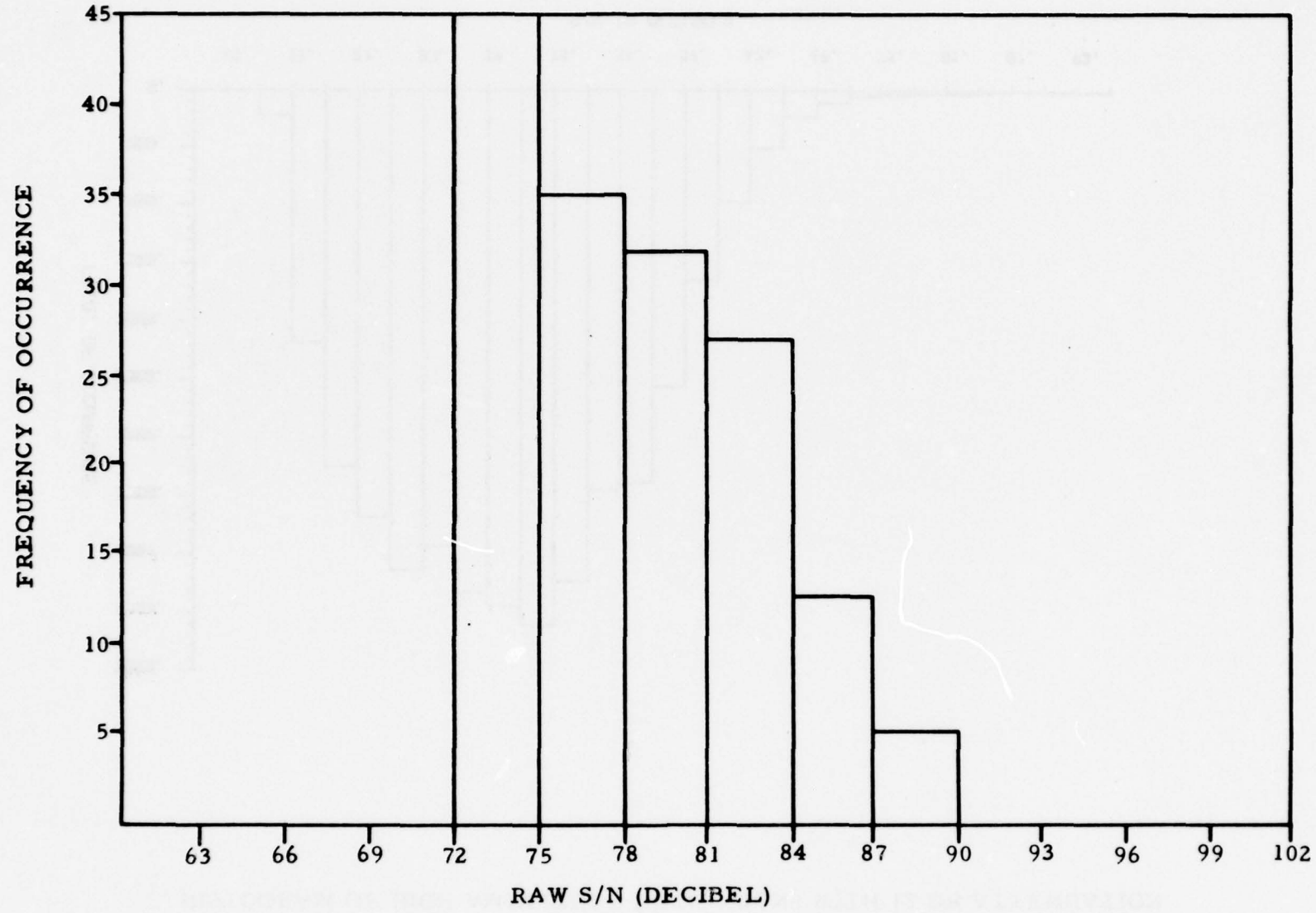

Figure 2-14

HISTOGRAM OF HIGH AMPLITUDE DETECTIONS WITH 12 dB ATTENUATION

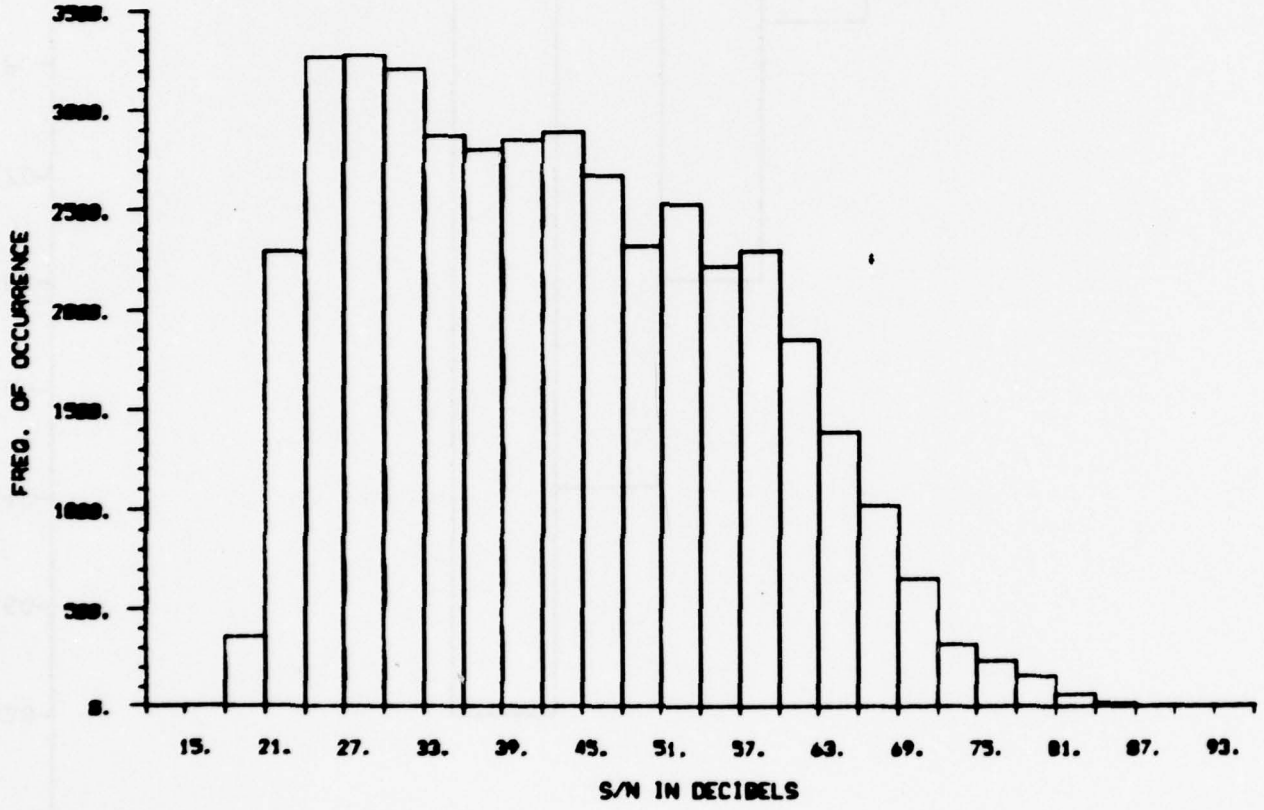

Figure 2-15

HISTOGRAM OF HIGH AMPLITUDE DETECTIONS
WITH 12 dB ATTENUATION (SCAN 793, 92/10/10/20)

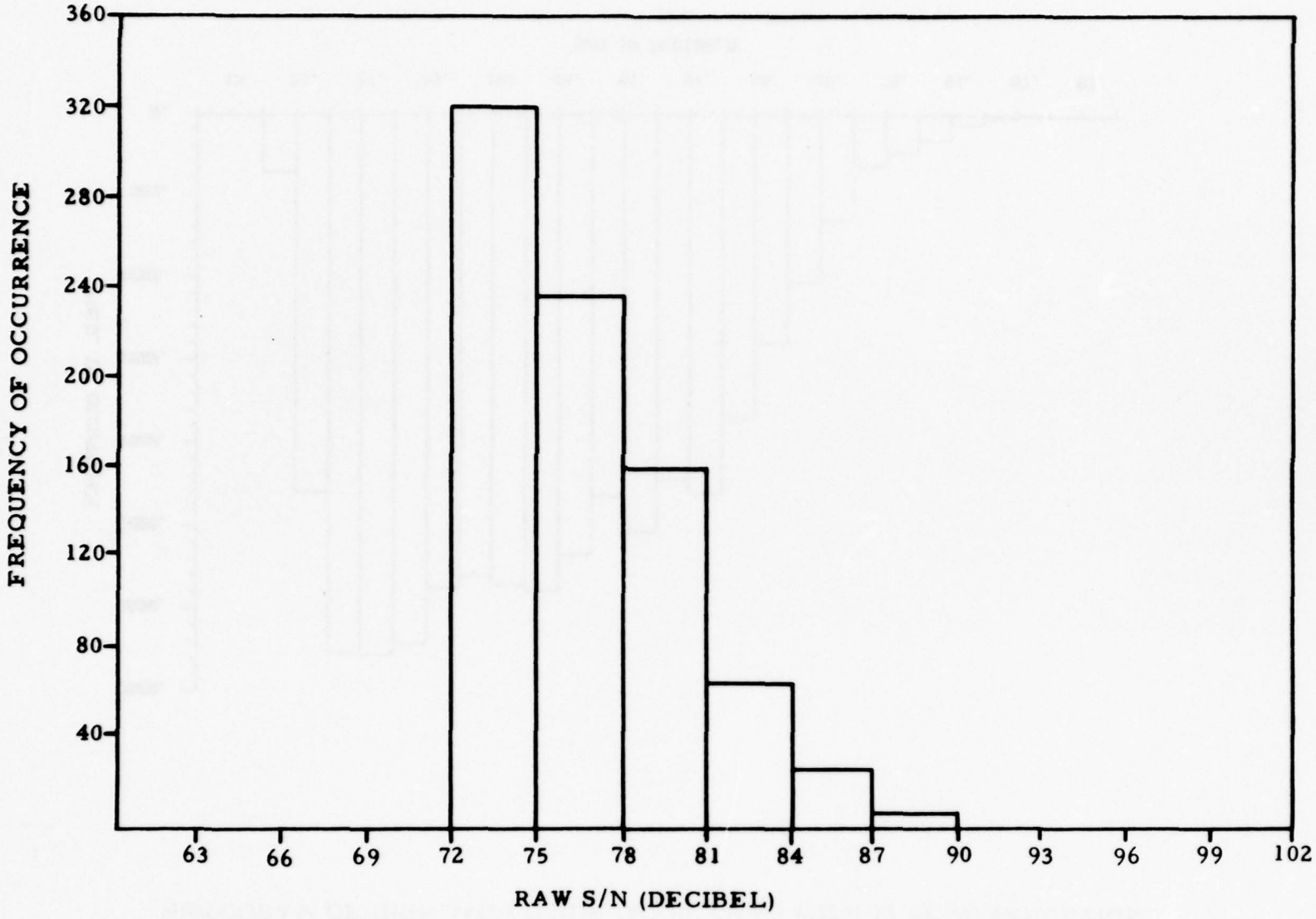

Figure 2-16

UNBLANKED GRATING LOBES SCANNING THE AURORAL REGION
(UNMODIFIED SUBARRAY)

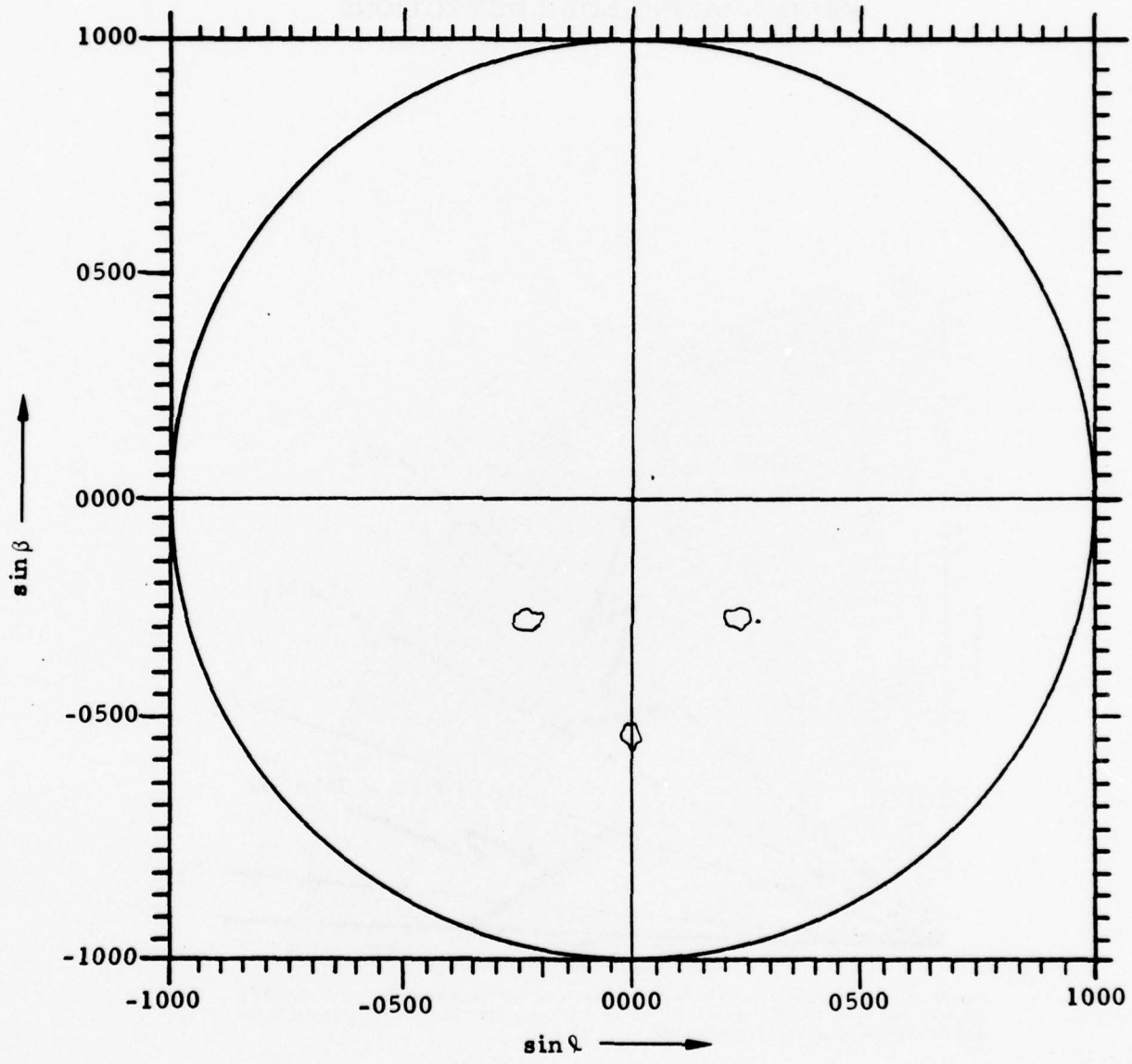

Figure 2-17

GRAPHIC PRESENTATION OF APPARENT AURORA RESULTING FROM GRATING LOBE DETECTIONS

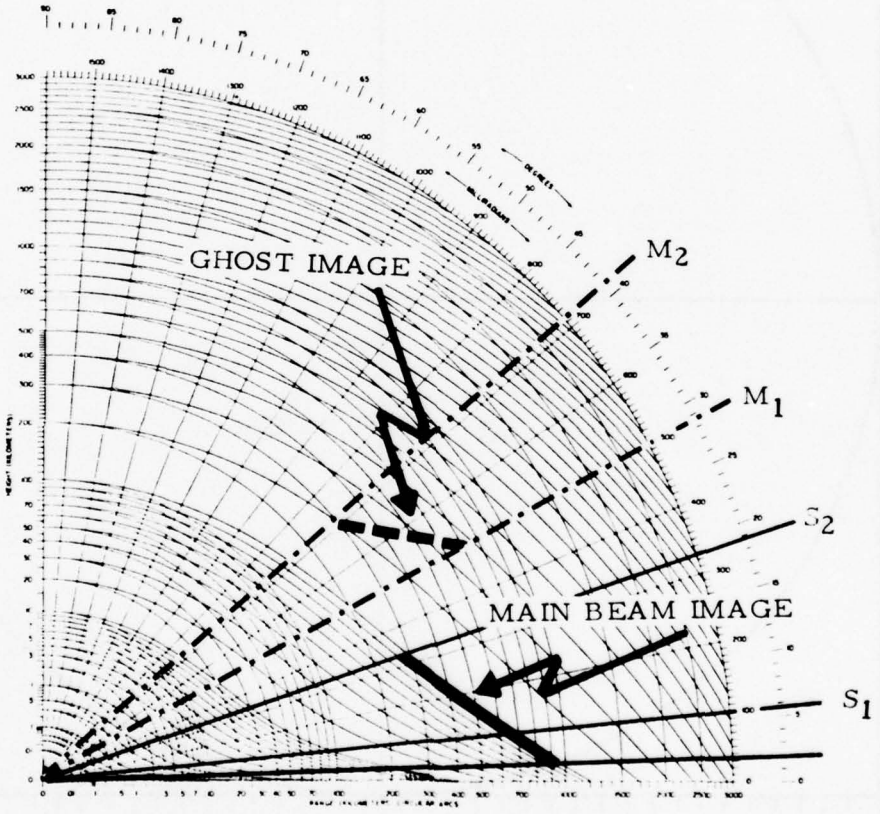

Fig. 29 Radar range-height-angle chart for targets to 3,000-km altitude. Calculated for straight ray lines, CRPL exponential reference atmosphere, $N_s = 313$; nonlinear range and height scales, and linear angle scale.

Figure 2-18

It is possible to use a histogram showing the distribution of the echo amplitude to gain some qualititive information about the echoes from the vestigial grating lobes. Figure 2-19 shows the unaveraged distribution of echo power from a single volume scan using echoes from the 100 to 110 km band. This effectively eliminates sidelobe echoes and the effects of beam-divergence (see Volume V, Section 3) [5]. These effects result in the addition of echoes of both medium and small amplitude. Echoes of intermediate amplitude are main beam echoes which did not originate at beam-center. The small echoes are mostly from the vestigial grating lobes. In both cases, these echoes appear to originate at altitudes other than that of the arc altitude of 105 to 106 km. The smaller or vestigial grating lobe echoes appear to originate up to very high altitudes. When the histogram is generated with data from all altitudes, as in Figure 2-20, the distribution of the additional echoes is immediately evident. By sampling only echoes which "appear" to come from far above the arc, as in Figure 2-21, only the medium and small echoes remain, and the peak from the vestigial grating lobes is readily apparent. At very high altitudes of 150 to 160 km, only the vestigial grating lobe echoes remain as shown in Figure 2-22.

The number of detections occurring due to the vestigial grating lobes depends upon the relative intensity of the auroral activity. During the measurement period on April 1, 1976, the global a_p Index exceeded 125, indicative of moderately intense auroral activity. For Scan 807, as many as 800 detections may have resulted from vestigial grating lobe illumination of the aurora. This would be equivalent to over 26 false detections per second. This would result in unnecessary data processor loading and, if some of these detections were to be verified, possible false tracks. The remainder would be nonverifiable and thus rejected, but would certainly cause the noise blanking threshold to be raised, reducing the sensitivity of the radar to all targets.

The ghost image just described has been observed in many of the auroral reflectivity maps generated as part of this study. An example is shown in Figure 2-23.

The overall effect of sidelobe blanking can be evaluated by turning off the Q-channel altogether. We find that removal of the Q-channel results in an increase of approximately 10 percent in the number of returns and a slight decrease of about 3 dB in the mean amplitude. This is a result of the Q-channel allowing low amplitude replies from the main beam and first sidelobes to appear. These will appear, when treated as main beam replies, to come predominately from the lower altitudes, which corresponds to smaller ranges and minimized beam broadening effects.

HISTOGRAM OF ECHO POWER FROM 109 to 110 KM BAND (SCAN 5387)

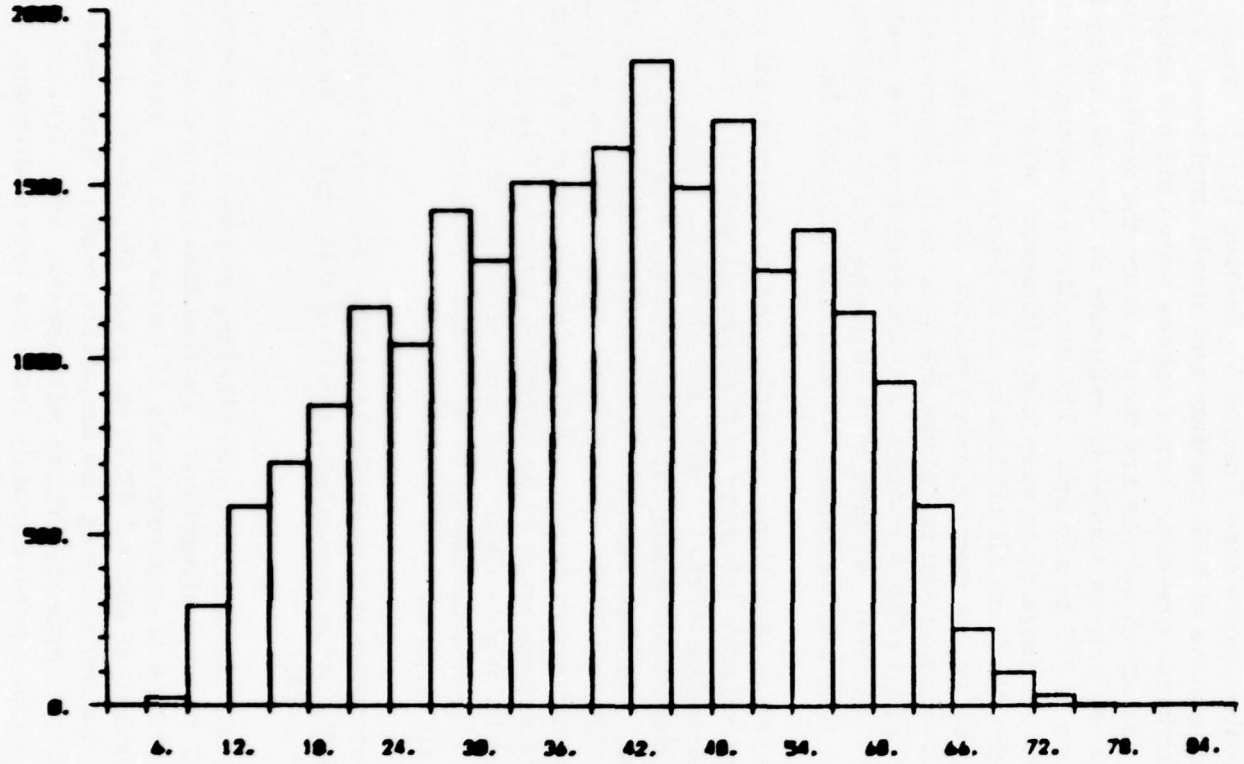

Figure 2-19

HISTOGRAM OF DETECTIONS USING DATA FROM ALL ALTITUDES (SCAN 5387)

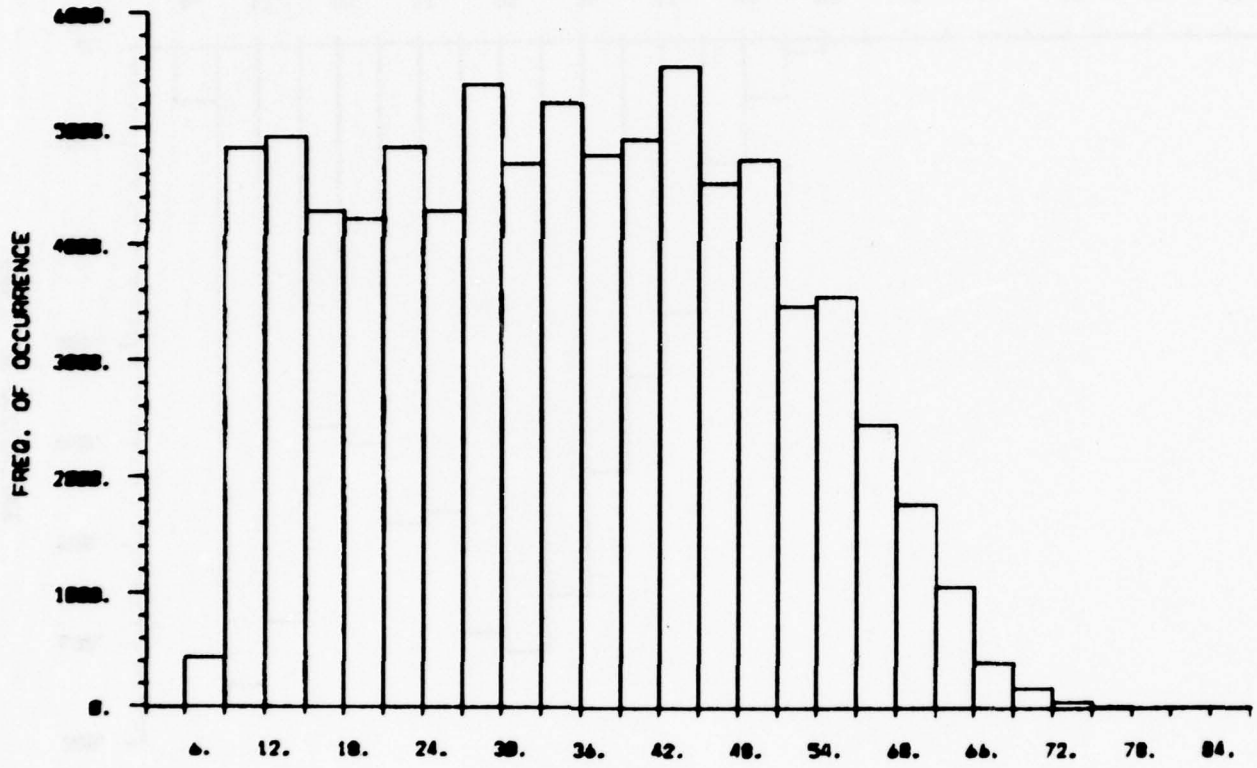

Figure 2-20

HISTOGRAM OF DETECTIONS FROM THE 130 TO 140 KM ALTITUDE BAND (SCAN 5387)

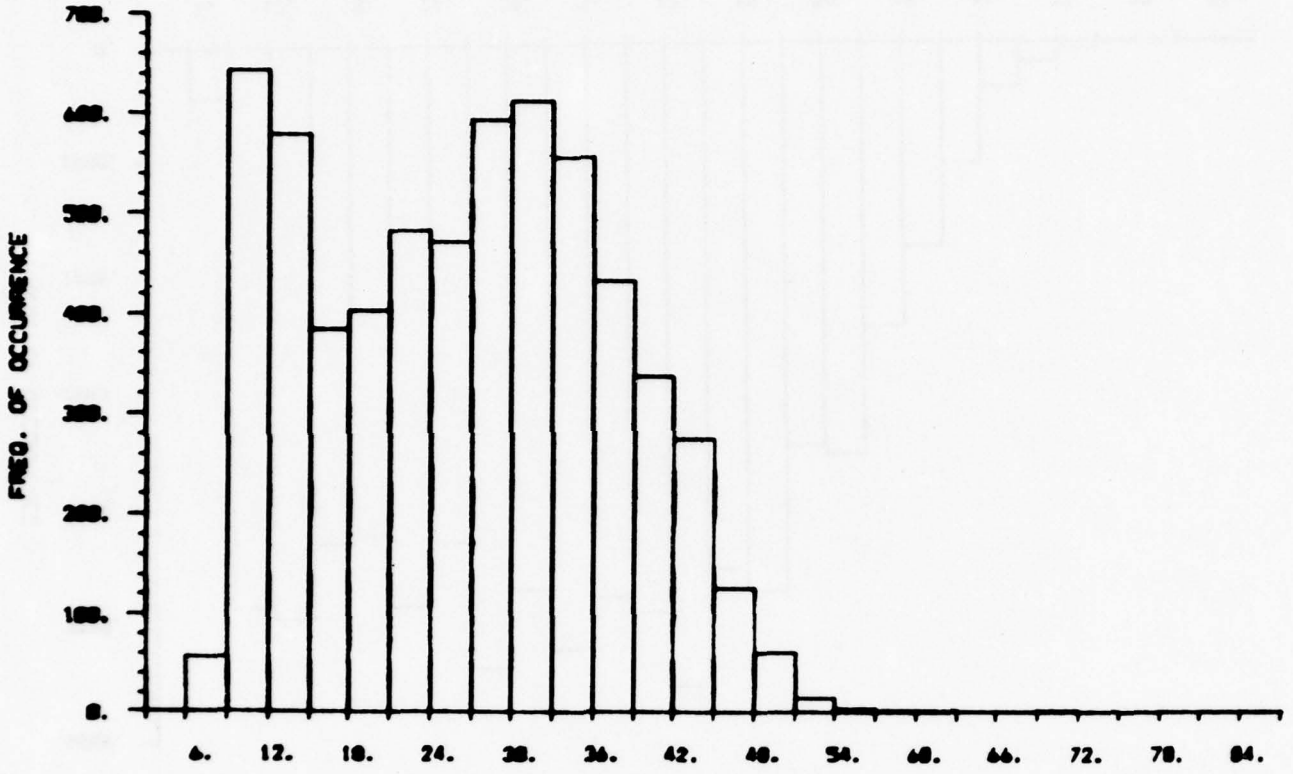

Figure 2-21

HISTOGRAM OF DETECTIONS FROM THE 150 TO 160 KM BAND (SCAN 5387)

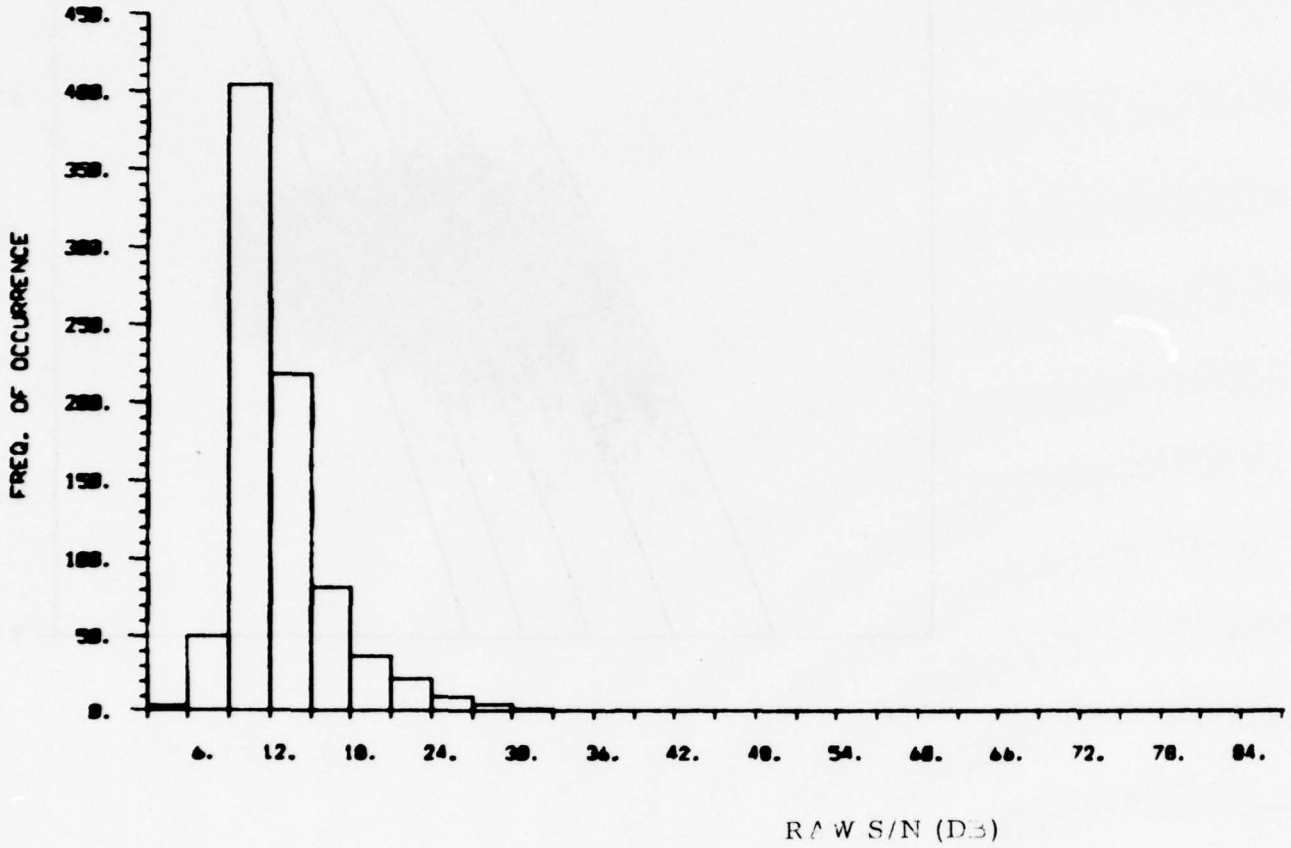

Figure 2-22

PROFILE VIEW OF AURORA PHENOMENA AT PAR (SCAN 665)

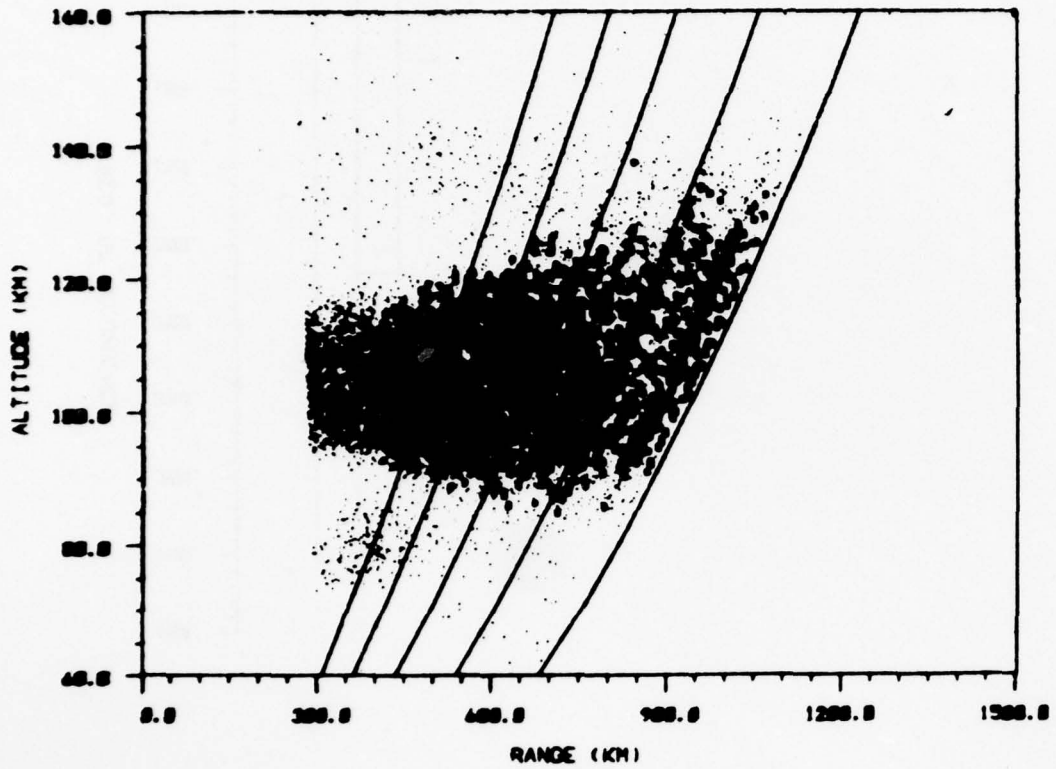

Figure 2-23

This is demonstrated in Figures 2-24 and 2-25 which show, respectively, a single beam trace for data with and without the Q-channel. The few replies, shown at low altitudes for the case where the Q-channel is in the system, result from the unavoidable statistical failures.

In addition to these replies, there are also replies which originate in the vestigial grating lobes shown in Figure 2-17. These returns appear only when there is an aurora sufficiently cose to the radar to be scanned under the corresponding conditions of low range attenuation and small off-broadside angle. Figures 2-26 and 2-27 are two examples of profile plots showing close-in sidelobe replies. Further demonstration that these replies are indeed due to the grating lobes can be achieved by examining previously discussed Figures 2-20, 2-21, and 2-22.

2.5 Conclusions From the Sidelobe Blanking Study

The sidelobe blanking study was performed primarily to analyze the effectiveness of phase tapering of the currently implemented Q-channel subarray pattern in blanking the 22 vestigial grating lobes present in the main beam patterns. Unfortunately, this part of the study could not be satisfactorily performed since the requisite addition of gain to the Q-channel receiver path was not performed. Nevertheless, the effectiveness of the unmodified Q-channel could be evaluated. There has been no attempt to recommend any specific changes to the PAR Q-channel, but only to point out a source of possible performance degradation due to the incomplete blanking performed by the existing configuration.

The primary effect of incomplete blanking is the presence of a ghost image of the aurora outside of the auroral exclusion volume. This results in a significantly elevated false alarm rate. The radar will attempt to compensate for this by raising its noise blanking threshold which in turn reduces its overall sensitivity. Further effects will be an increase in data processor loading, the possibility of attempted tracks, and blinding the radar to certain angles because of an excessive number of sidelobe detections.

SINGLE BEAM TRACE FOR DATA WITH Q-CHANNEL IN SYSTEM

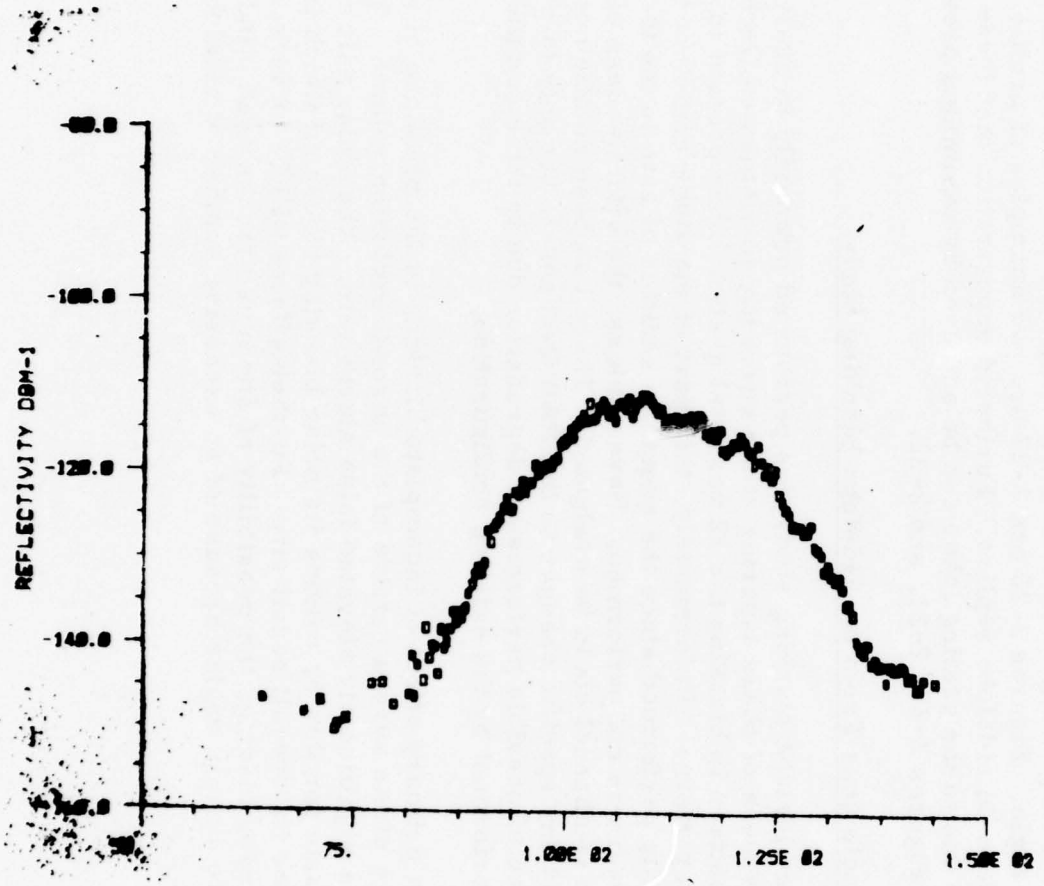

Figure 2-24

SINGLE BEAM TRACE FOR DATA WITH Q-CHANNEL OUT OF SYSTEM

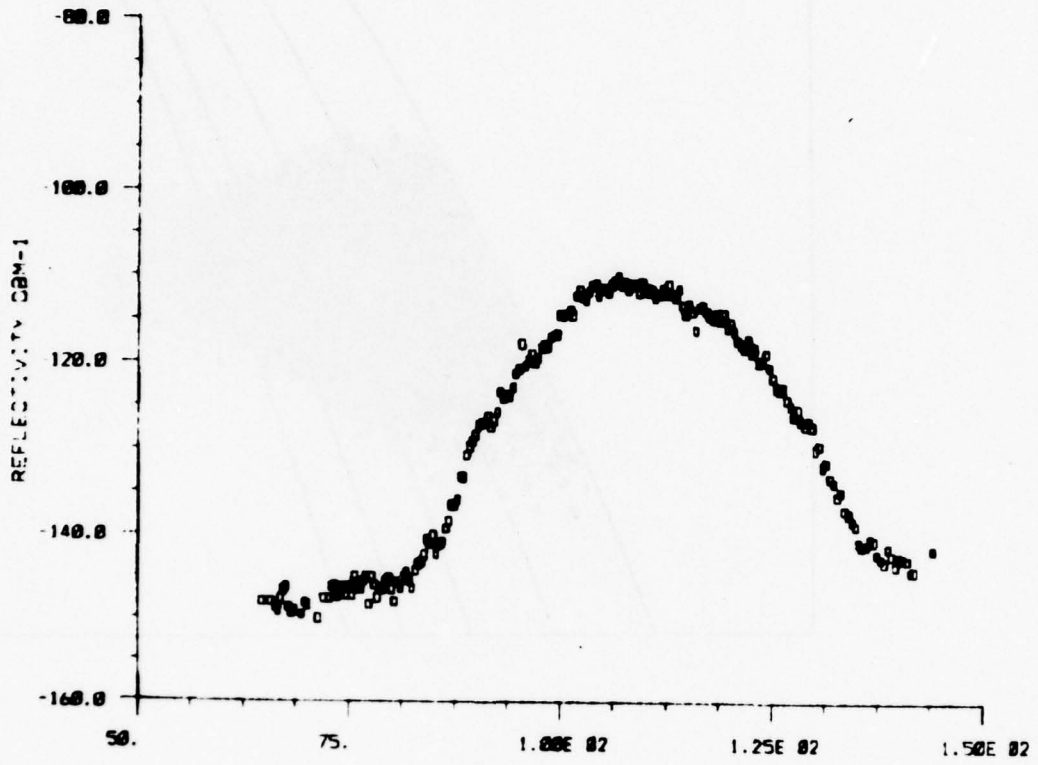

Figure 2-25

PROFILE VIEW SHOWING CLOSE-IN SIDELOBE REPLIES (SCAN 520)

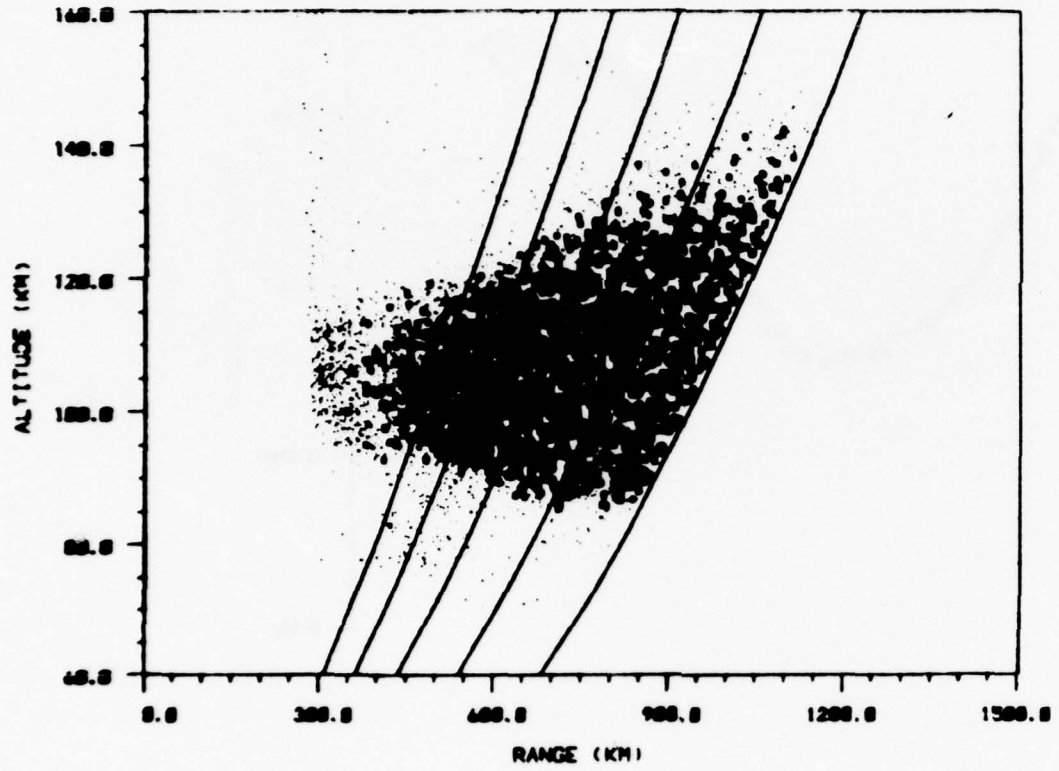

Figure 2-26

PROFILE WITH NO Q-CHANNEL SHOWING CLOSE-IN SIDELOBE REPLIES (SCAN 2198)

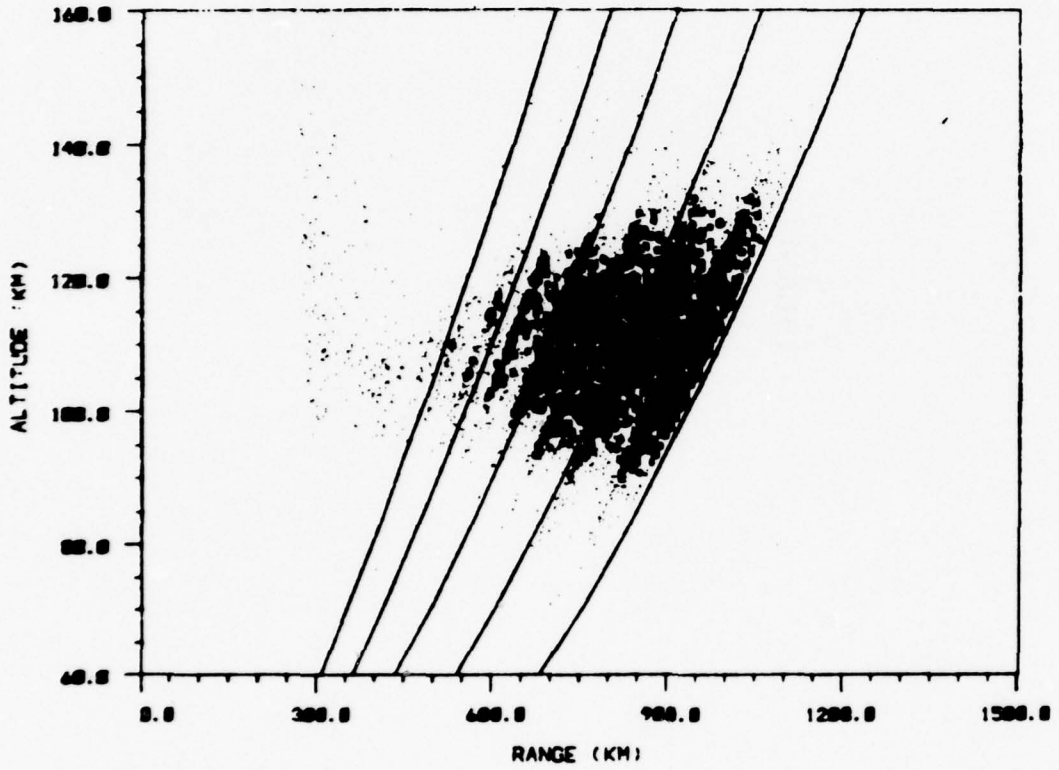

Figure 2-27

3. THE EFFECTS OF AURORALLY GENERATED NOISE IN THE PAR FREQUENCY BAND

One of the objectives of the PAR Auroral Study was to determine the chracteristics of aurorally generated noise in the PAR frequency band. The primary goal was to determine whether there was enough of this noise to significantly degrade the sensitivity of the radar. Additional study tasks included efforts to determine the spatial characteristics of any existing noise sources with respect to geomagnetic parameters and to determine whether or not the amplitude of this noise was related to the level of geomagnetic and auroral activity. The data collection process consisted of stepping through the normal auroral raster scan with the transmitters turned off. Any measured video peak would result from a combination of receiver noise, normal background sky noise, and auroral noise. A noise threshold is used in the signal processor to eliminate video peaks which are below 10 dB s/n. Video peaks which pass this threshold will be converted to digital format, and recorded on magnetic computer tape for off-line processing.

Satellite observations of VLF radiation in the upper atmosphere in polar regions have provided a wealth of material regarding VLF radio noise generation. The scarcity of documented evidence relating to UHF radio emissions from the aurora suggests that the aurora generates little noise in the UHF range. An increase in noise level at the radar can occur even if this noise is not generated by the aurora. The detected energy can result from the reflections of signals from other sources operating in the same band, and these bi-static reflections may be misinterpreted as radio emissions originating from the auroral region.

The following discussion presents the methodology of data collection and analysis results. The experiment to sample possible radio noise emanations from the aurora was designed to provide a cold-sky reference in order to establish the normal background count of video peaks. This reference level would be used later for comparison with measurements taken during auroral activity. Measurements were to be taken several times throughout the experiment, during periods of quiet auroral activity, and during the apparent peak of auroral activity. The video peaks detected during these measurements were recorded digitially on magnetic data tapes for off-line reduction and analysis. Noise measurements were made on the nights of March 26, 1976, and April 1, 1976.

3.1 Reference Noise Measurement

The reference measurement was taken using the Special Search (SPSE) function of the aurora software module.

The SPSE function executes 54 beam raster centered at a user-specified pointing angle. Unlike the full aurora raster, the SPSE raster may be positioned

anywhere within allowable visible space. Once initiated, the SPSE raster continues to scan a six-beam-by-nine-beam volume until it is manually terminated.

Note: The aurora software module is a specially modified version of the tactical process which normally drives the PAR. Descriptions of the modifications are provided in Volume I. Additional modifications were required for the Spring 1976 experiment and are detailed in Volume III.

For this measurement, the center of the 54 beam SPSE raster was steered to sine space coordinates $\alpha = 0$, $\beta = .5000$ (toward geomagnetic north at an elevation angle of about 55°). Using a 10 dB s/n threshold, data was collected for approximately 2 minutes, providing a sample of 192 scans of .66-seconds duration each. Analysis of this data indicated a mean detection (noise return) rate of 1.5 per second. The data yielded the expected Rayleigh distribution similar to that shown by the Histograms in Figures 3-1 through 3-3. It can be seen that a number of measurements showed peaks below the 10 dB noise threshold. This can be attributed to analog-digital converter switching response lag.

3.2 Measuring the Auroral Noise

Several times throughout the night of March 26, 1976, and again on April 1, 1976, noise measurements were made using both the 54 beam SPSE raster and the full aurora scan raster. The transmitter was inhibited during these measurements. The SPSE raster was centered at sine space coordinates $\alpha = .0138$, $\beta = -.3151$ (roughly north at about 4° elevation). The aurora raster scanned left-to-right, bottom-to-top from 2° to 20° elevation. Data obtained during these measurements was recorded on magnetic tape for off-line reduction.

3.3 Data Analysis

The primary off-line reduction resulted in the generation of plots of sine space coordinates versus maximum intensity of returns detected at each coordinate. It was believed that if the aurora indeed emanated noise in the PAR band, localization of video detections in sine space coordinates might be evident. A complicating factor in the analysis of noise returns is the possibility of bi-static reflections which would also be evidenced by localization of detected video peaks. Further complications may be caused by the presence of radio stars, such as Cassiopea Alpha and Cygnus Alpha, in the field of view.

Figure 3-4 shows the resulting superposition of 172 SPSE volume scans taken on Marsh 26, 1976, form 0423 u.t. to 0425 u.t. The density of the plot

HISTOGRAM REPRESENTING NOISE RETURNS
FROM COLD SKY MEASUREMENT
MARCH 26, 1976

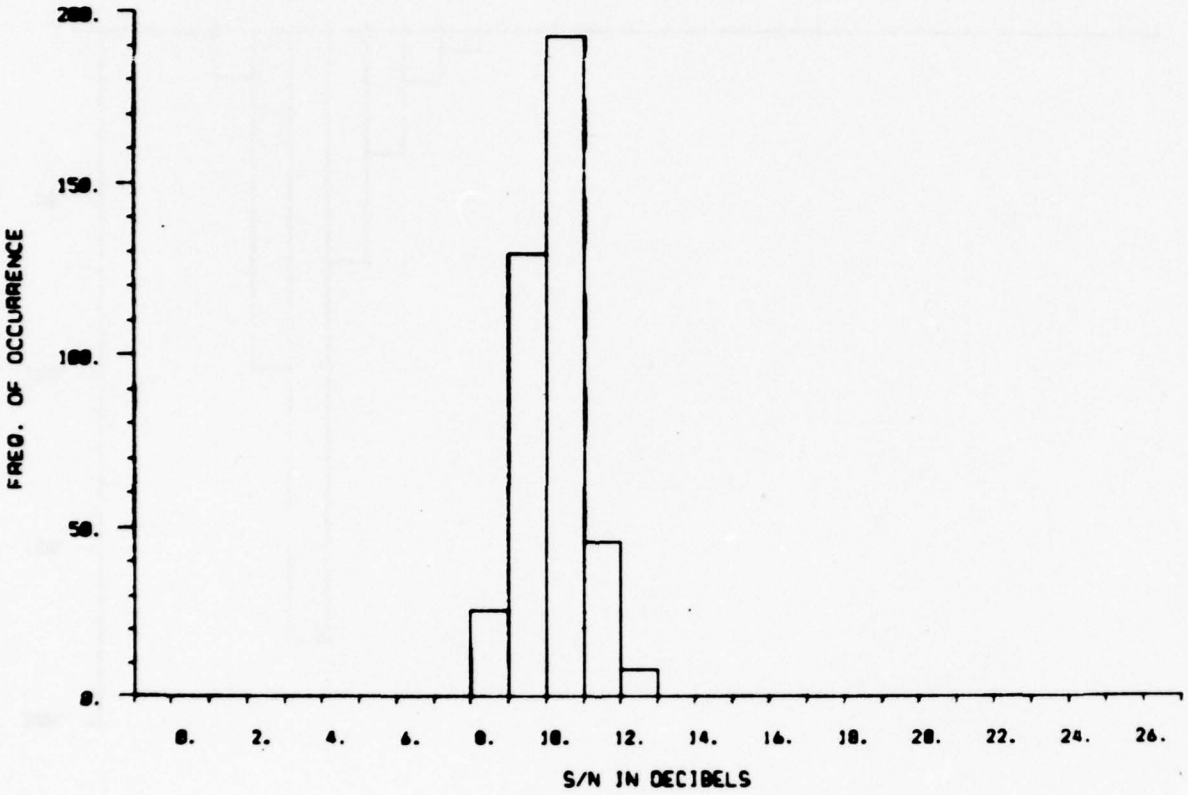

NOISE DISTRIBUTION - QUIET SKY

Figure 3-1

HISTOGRAM REPRESENTING NOISE RETURNS
DURING RF INHIBIT
MARCH 26, 1976

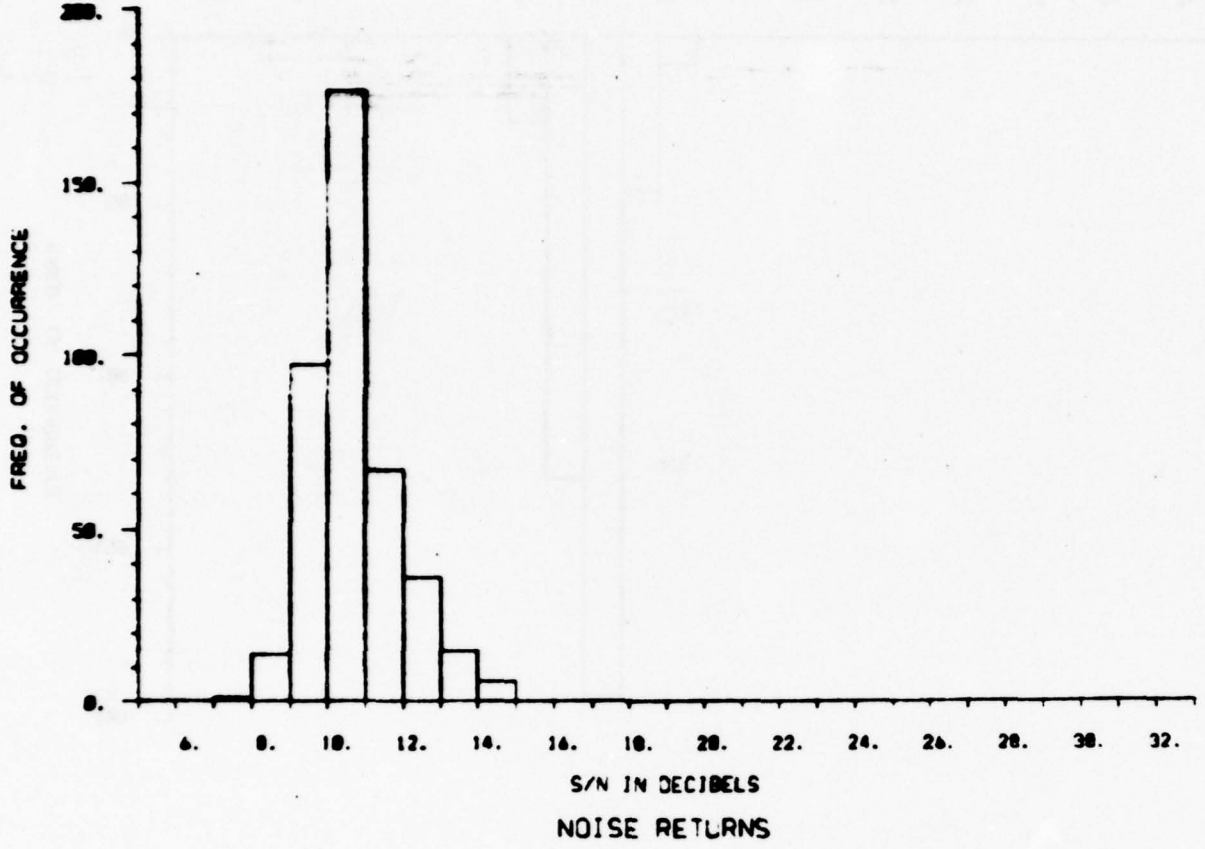

Figure 3-2

HISTOGRAM REPRESENTING NOISE RETURNS
DURING RF INHIBIT
APRIL 1, 1976

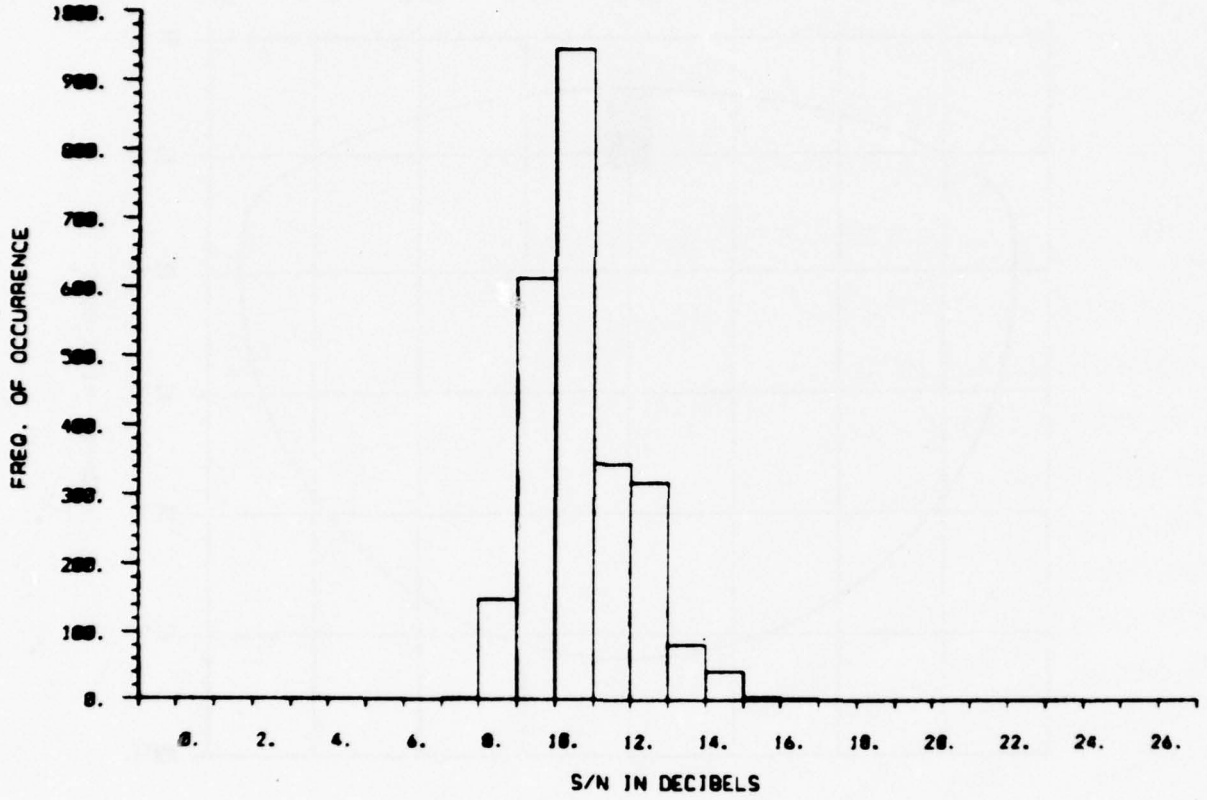

NOISE DISTRIBUTION DURING RF INHIBIT

Figure 3-3

SUPERIMPOSITION OF 172 SPSE VOLUME
SCANS DURING RF INHIBIT
MARCH 26, 1976

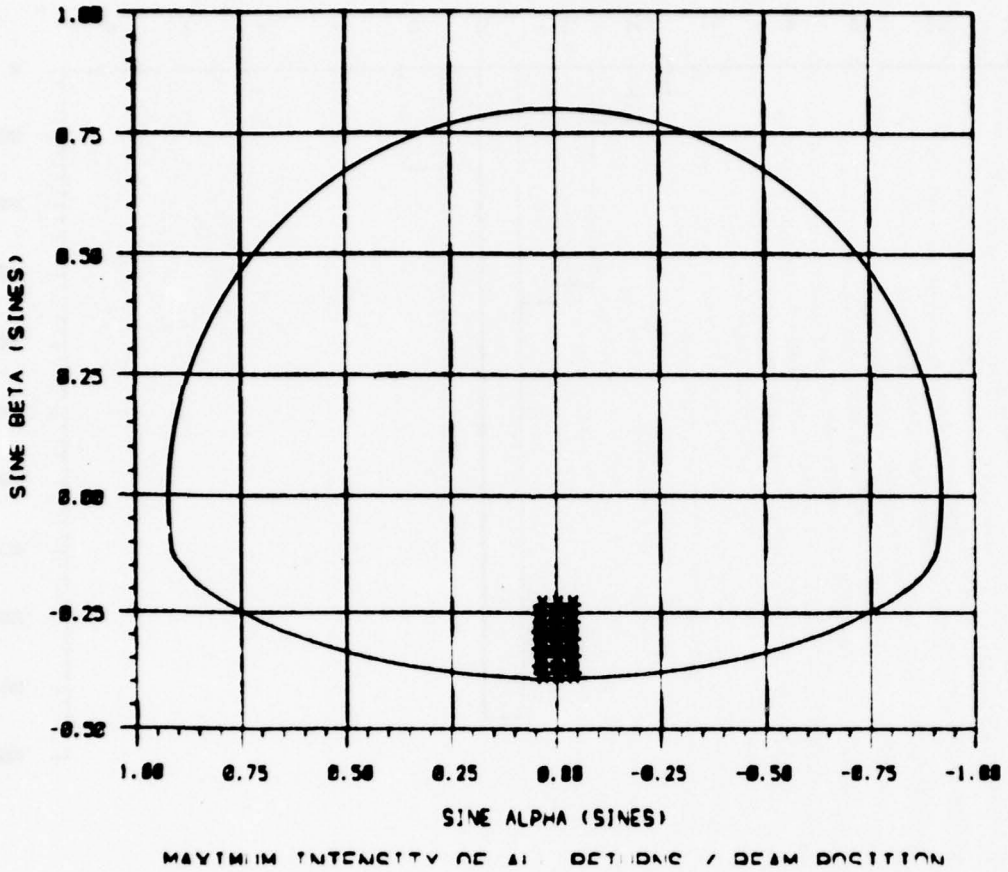

Figure 3-4

would at first suggest intense noise generation, but the average detection rate for the 2-minute period was only four per second. Table 3-1 provides a tabulation of the noise measurements made on March 26, 1976. The raster implemented for data collection is indicated by S(SPSE) or N (full aurora scan) in the second column. For each SPSE collection period, the sine space coordinates of the raster center are provided. Additional tabulated data included the number of scans executed during the data collection period, the mean number of detections per scan and per second (sum of both beams), the manual setting of the signal threshold, and the relative activity of the aurora as a function of the number of backscatter detections encountered prior to, and immediately following, the noise measurement. Of particular interest is the decreasing average per scan return rate of the SPSE scans as the apparent intensity of the aurora increases. This phenomenon may be due to increased auroral absorption of electromagnetic waves from the cosmic noise sources effectively masking the noise level, or at least reducing the intensity such that is falls below the established 10 dB noise threshold. There is insufficient data from full-raster scans during relatively quiet aurora to make a valid comparison.

Figures 3-5 through 3-11 show the auroral reflecting regions at approximately the times the noise measurements were made. The smaller SPSE scan from which the analysis was made was limited by the boundaries shown in these figures.

Figures 3-12 through 3-15 present a sample of four contiguous scans using the full raster. (Note the apparent localization of returns in the right-hand portion of the plot.) Comparison of the average per second return rate of these scans (7.2) with the much smaller SPSE raster (1.2 to 3.6) provides little additional information since the full raster may detect signals from radio stars as well as reflections from other sources which may not be detected by the 54 beam SPSE raster.

The data reduced from the experiment conducted on April 1, 1976, produced similar results. The returns exhibited a Rayleigh-like distribution as was shown previously in Figure 3-2. The tabulated data from the noise measurements for the full-raster scans are provided in Table 3-2. It should be noted that the level of the signal blanking threshold was varied several times throughout the experiment, ranging from a low of 6 dB to a high of 10 dB. The increase in the total number of returns per scan is directly attributable to the decrease in threshold. This effect should, however, be fairly uniform over the entire scan.

Composites of several full-raster scans were prepared to determine if any localization of returns could be seen. Figure 3-16 shows a composite of three scans covering nearly 90 seconds. The composite shows apparent localization of returns at sine space coordinate $\alpha = -.25$ to $-.35$, $\beta = .0$ to $.10$,

AURORA NOISE MEASUREMENTS

Date/Time	Raster	Sin α	Sin β	#Scans	Mean # Returns Per Scan	Mean # Returns Per Sec	Noise Threshold	Auoral Activity (# Returns)	
								Before	After
86/04/23/05.0	S	.0138	-.1377	173	4.9	7.4	10 dB	16K	20K
86/04/25/19.5									
86/04/50/30.0	S	.0138	-.3051	87	4.1	6.2	10 dB	20K	34K
86/04/51/27.5									
86/06/07/06.0	S	.0138	-.3051	86	3.07	4.6	10 dB	38K	38K
86/06/08/02.5									
86/06/31/00.5	S	.0138	-.3051	90	2.92	4.4	10 dB	25K	50K
86/06/31/59.5									
86/07/04/07.0	N	FULL VOLUME		4	407.7	14.3	10 dB	57K	67K
86/07/05/59.5									
86/09/08/01.0	S	.0138	-.3051	128	1.7	2.6	10 dB	52K	85K
86/09/09/26.0									
86/09/13/34.5	N	FULL VOLUME		2	232	8.1	10 dB	85K	85K
86/09/14/30.5									
86/10/19/17.0	N	FULL VOLUME		9	66	2.3	10 dB	83K	83K
86/10/24/27.5									
86/10/41/00.0	S	.0138	-.3051	90	2.2	3.3	10 dB	73K	75K
86/10/41/59.0									

* S=SPSE N= NORMAL AURORA RASTER

Table 3-1

TOP-DOWN REFLECTIVITY MAP OF SCAN 1650

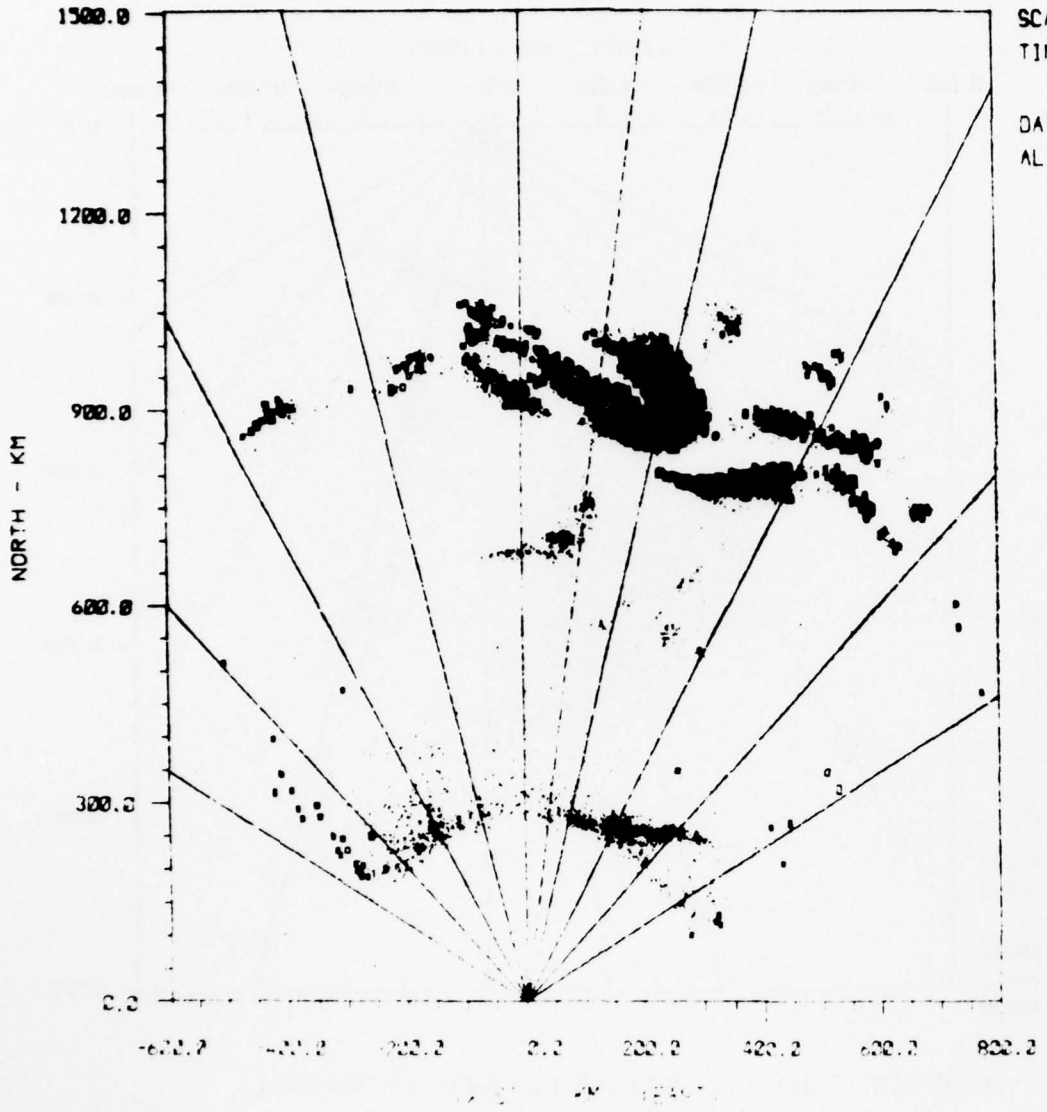

BEAM: BOTH
SCAN: 1650
TIME: FROM 86/ 4/40/50
TO 86/ 4/41/10
DATA THINNING FACTOR: 0
ALT (KM): 70.0 TO 170.0

ALTITUDES			ON LEVEL
70.0	TO	80.0 KM	5
80.0	TO	90.0 KM	6
90.0	TO	100.0 KM	7
100.0	TO	110.0 KM	8
110.0	TO	120.0 KM	9
120.0	TO	130.0 KM	10
130.0	TO	140.0 KM	11
140.0	TO	150.0 KM	12
150.0	TO	160.0 KM	13
160.0	TO	170.0 KM	14

Figure 3-5

TOP-DOWN REFLECTIVITY MAP OF SCAN 2809

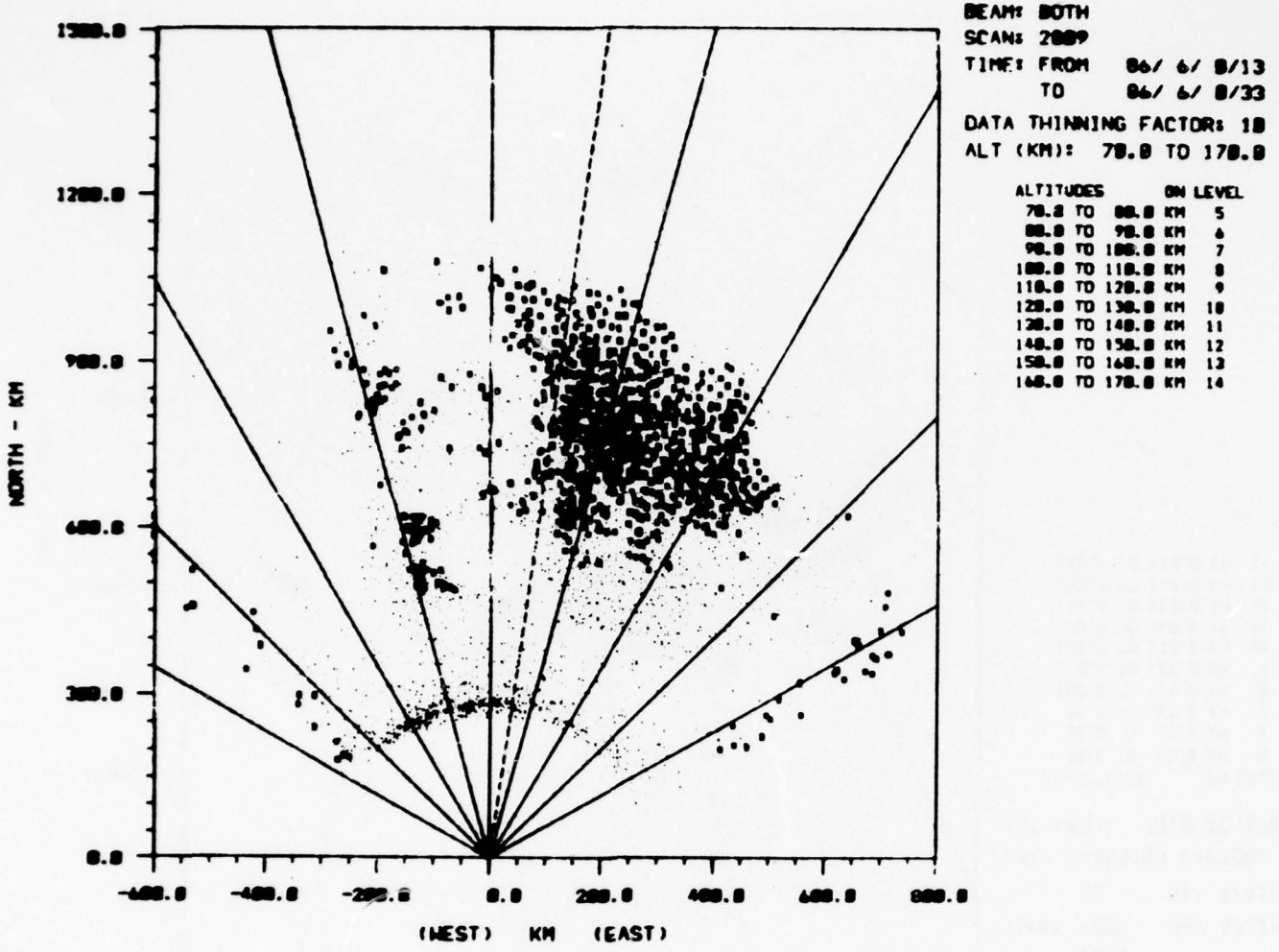

Figure 3-6

TOP-DOWN REFLECTIVITY MAP OF SCAN 3036

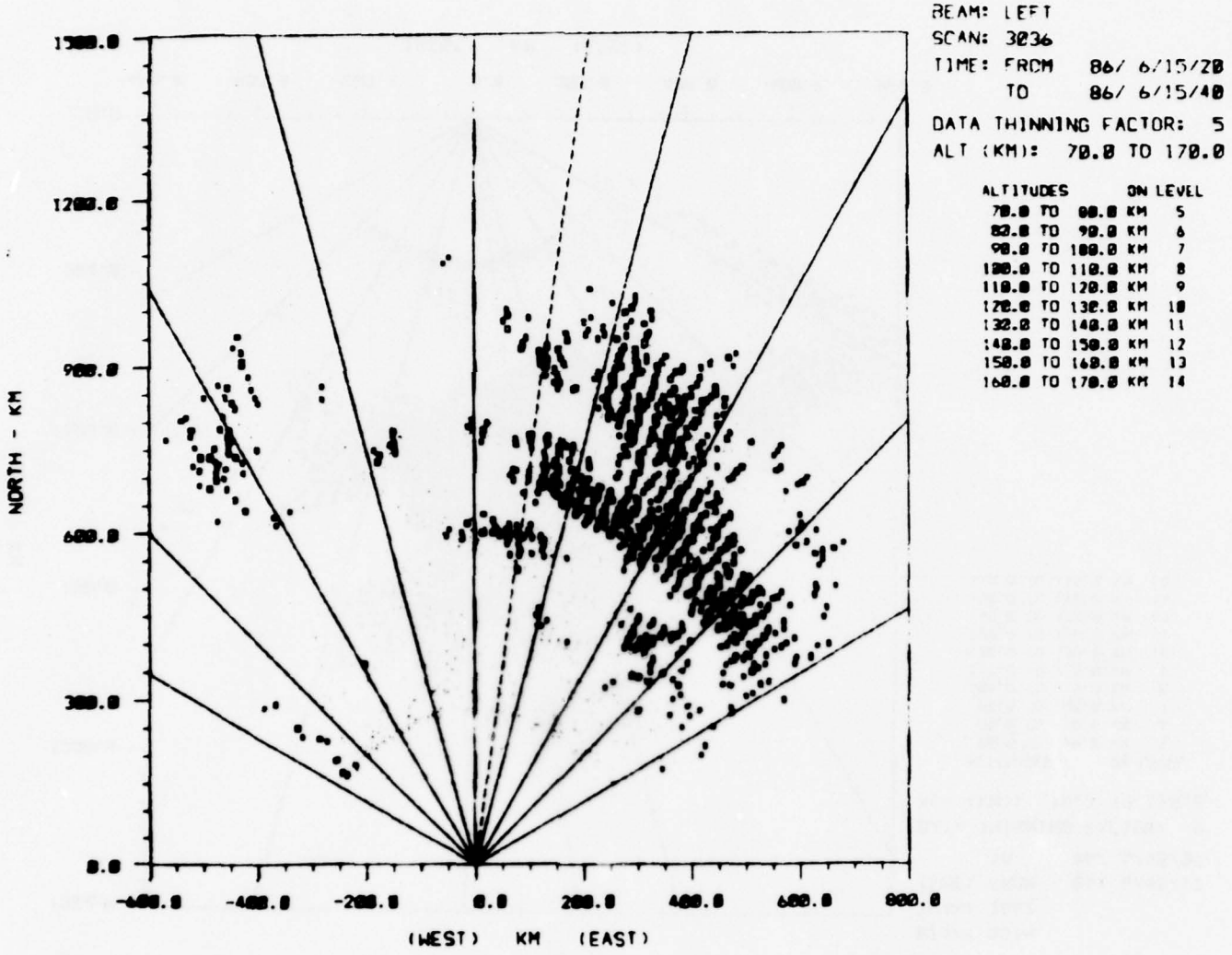

Figure 3-7

TOP-DOWN REFLECTIVITY MAP OF SCAN 3662

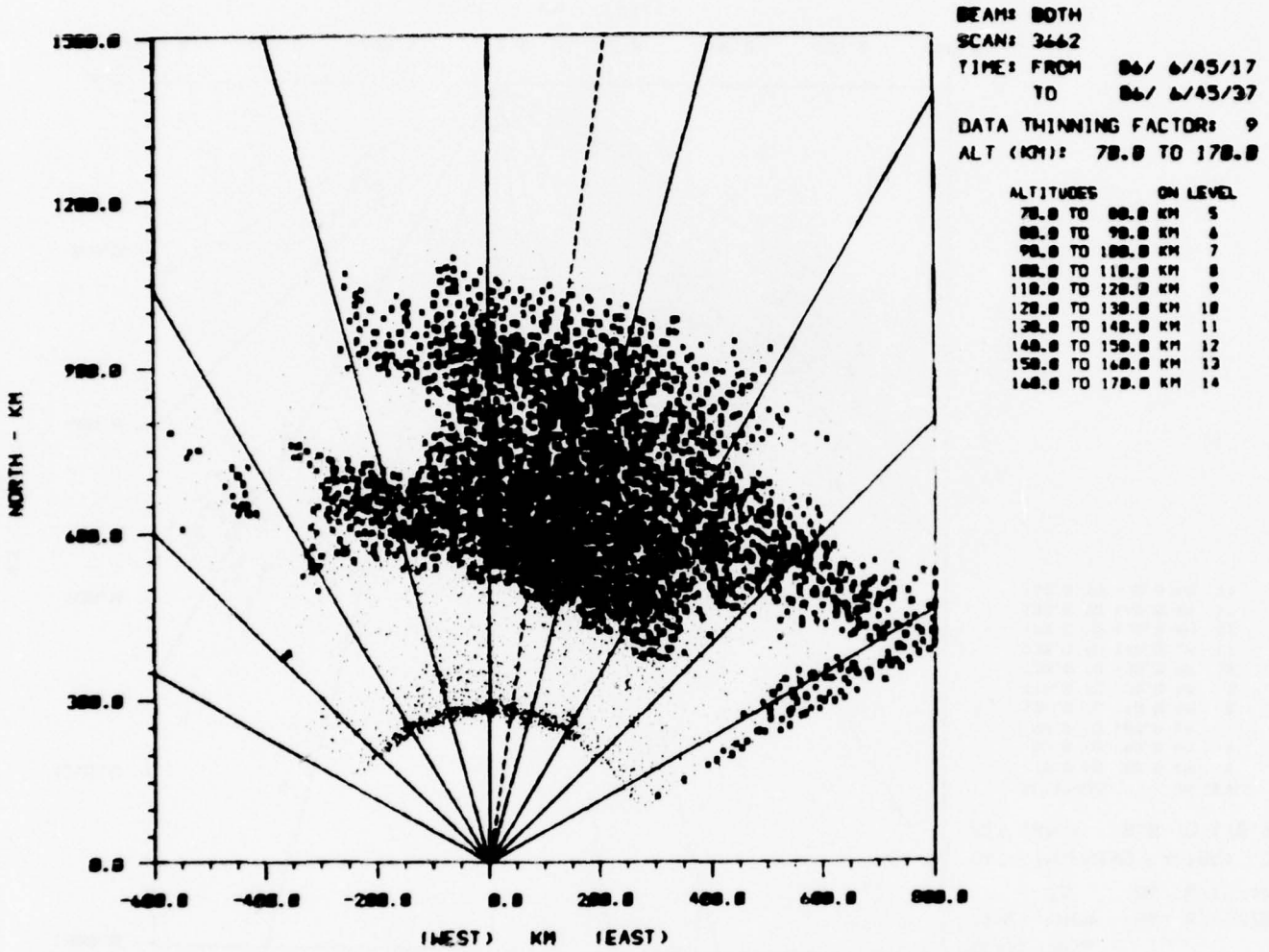

Figure 3-8

TOP-DOWN REFLECTIVITY MAP OF SCAN 4060

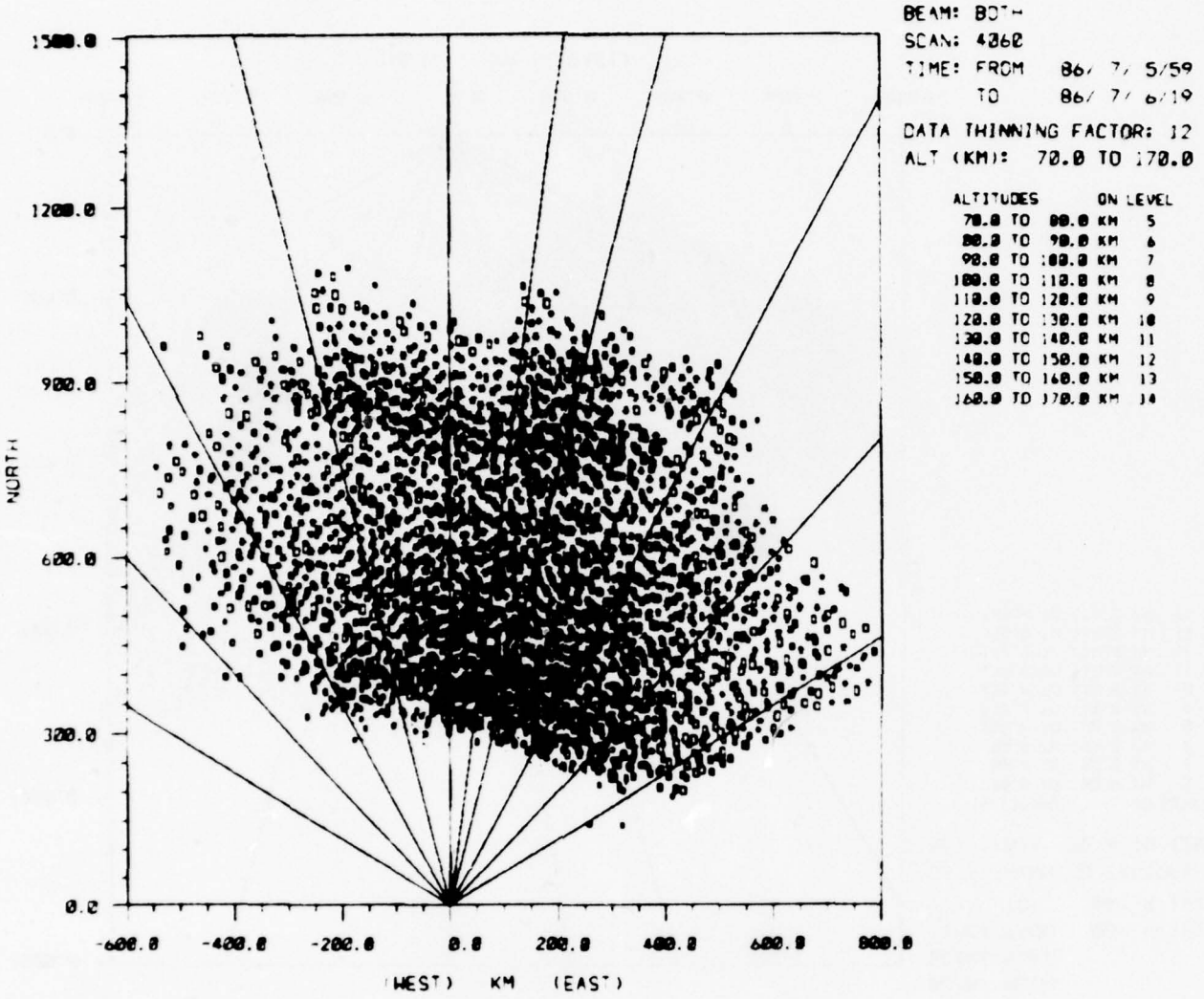

Figure 3-9

TOP-DOWN REFLECTIVITY MAP OF SCAN 5381

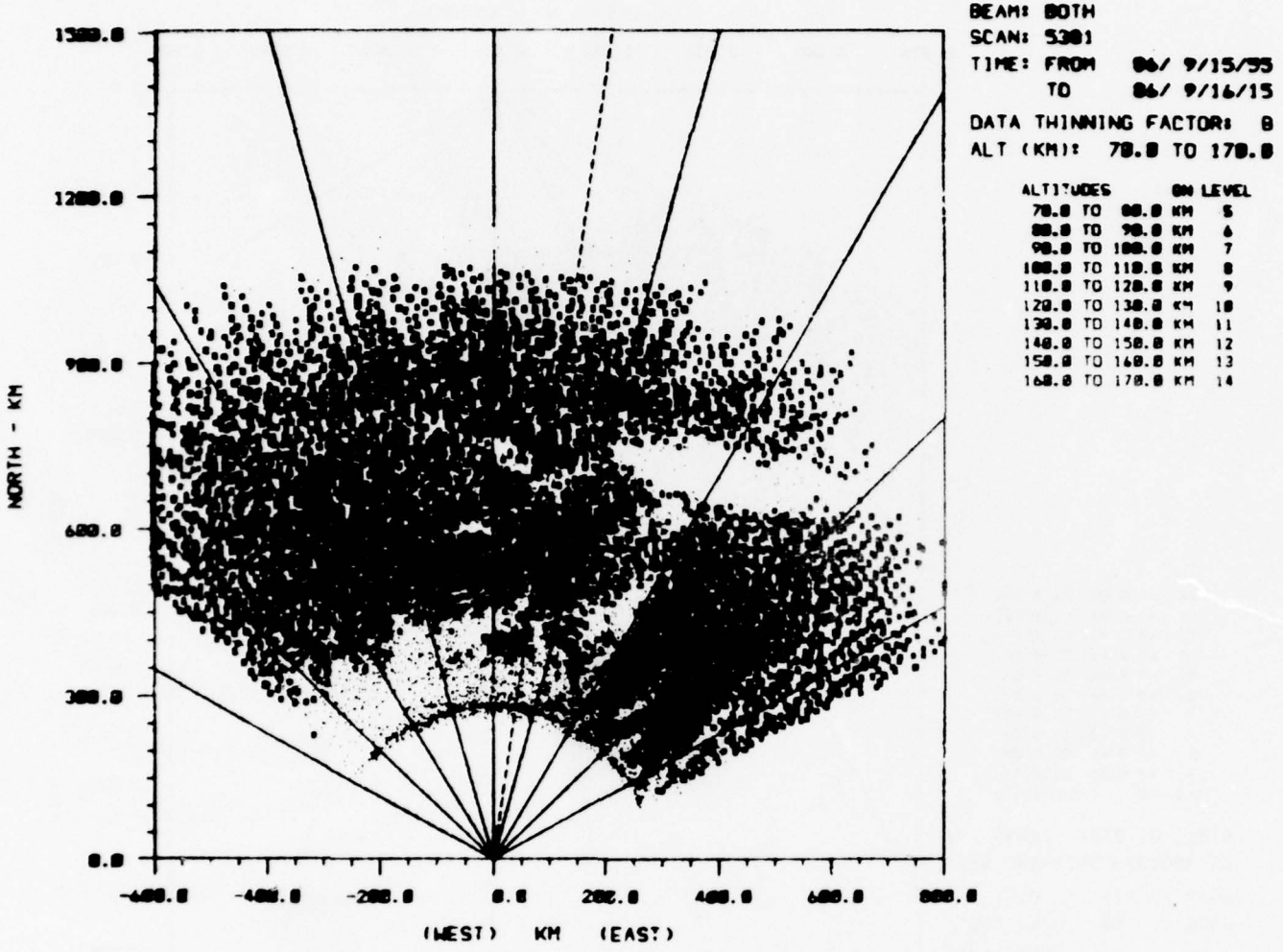

Figure 3-10

TOP-DOWN REFLECTIVITY MAP OF SCAN 5887

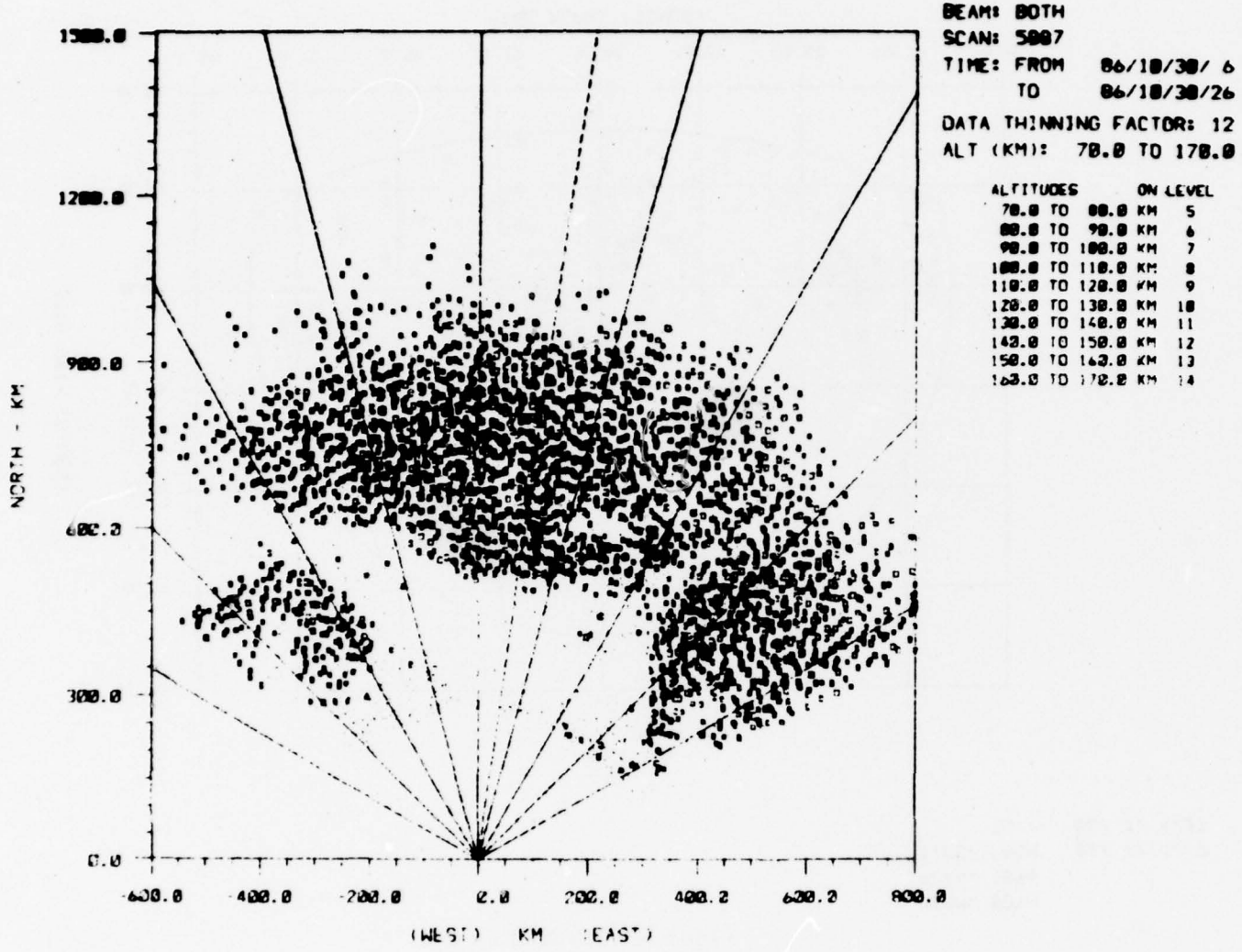

Figure 3-11

SINE SPACE PLOT SHOWING MAXIMUM
INTENSITY OF ALL RETURNS/BEAM
POSITION (SCAN 4056)

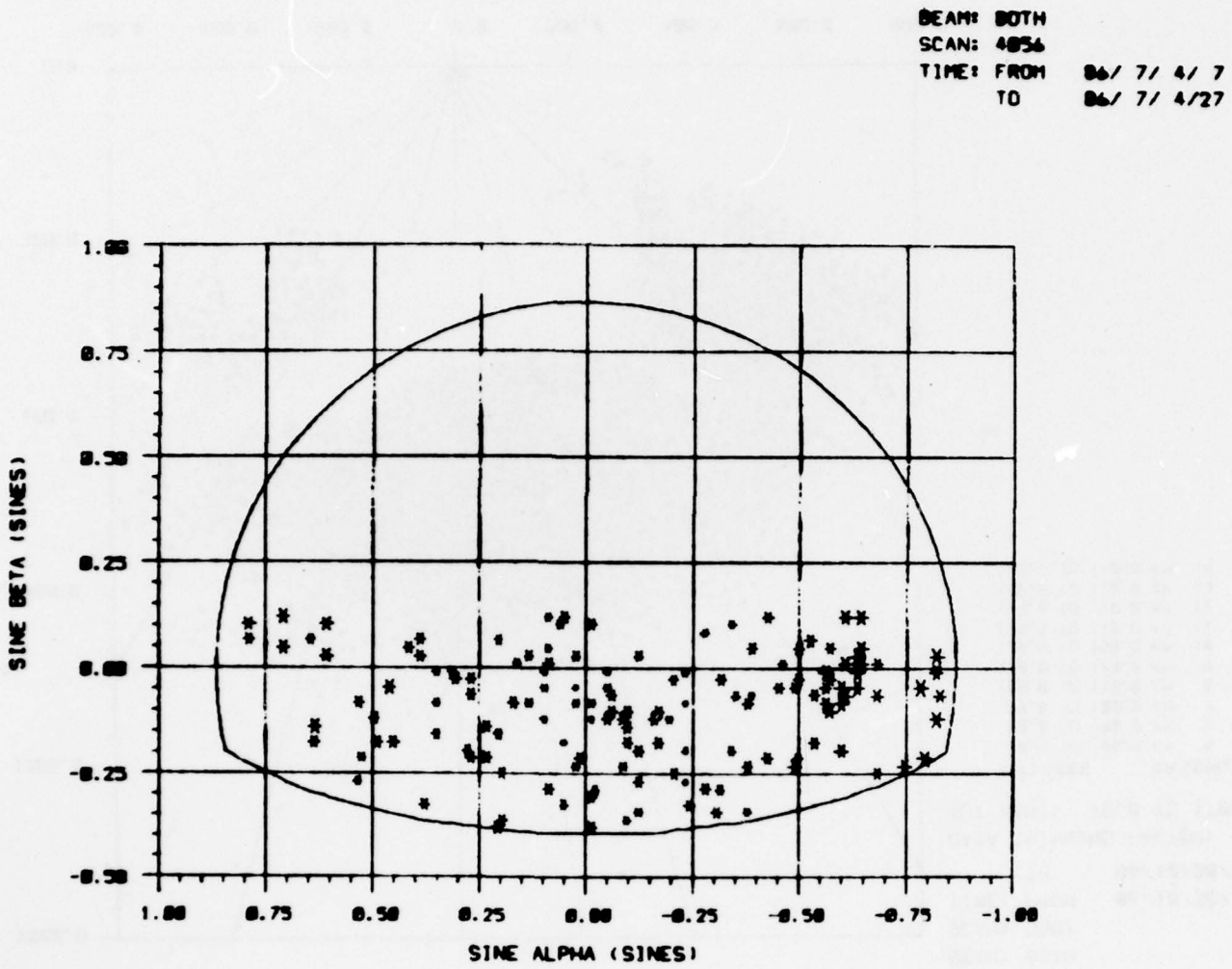

Figure 3-12

SINE SPACE PLOT SHOWING MAXIMUM
INTENSITY OF ALL RETURNS/BEAM
POSITION (SCAN 4057)

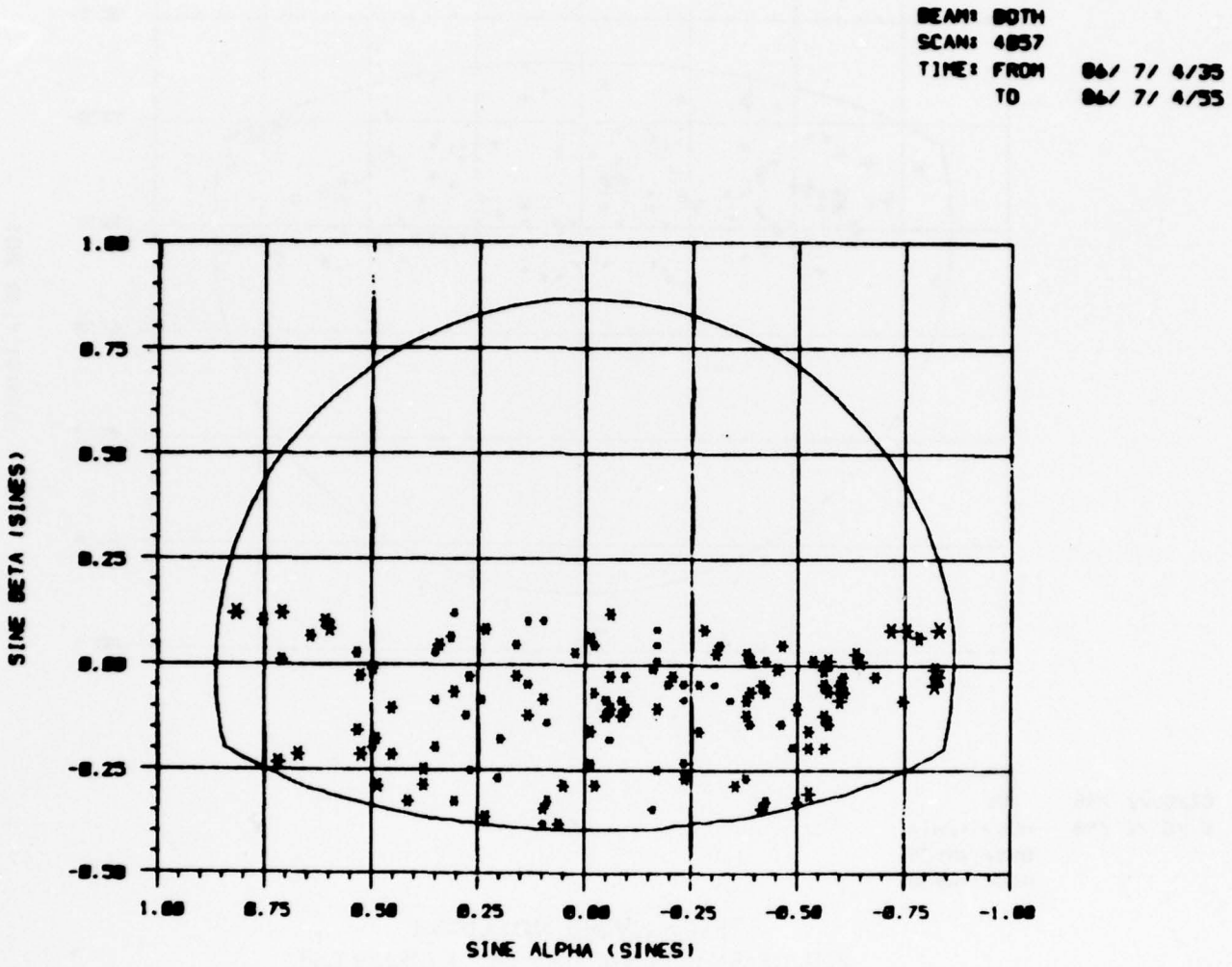

Figure 3-13

SINE SPACE PLOT SHOWING MAXIMUM
INTENSITY OF ALL RETURNS/BEAM
POSITION (SCAN 4058)

BEAM: BOTH
SCAN: 4058
TIME: FROM 86/ 7/ 5/ 3
TO 86/ 7/ 5/23

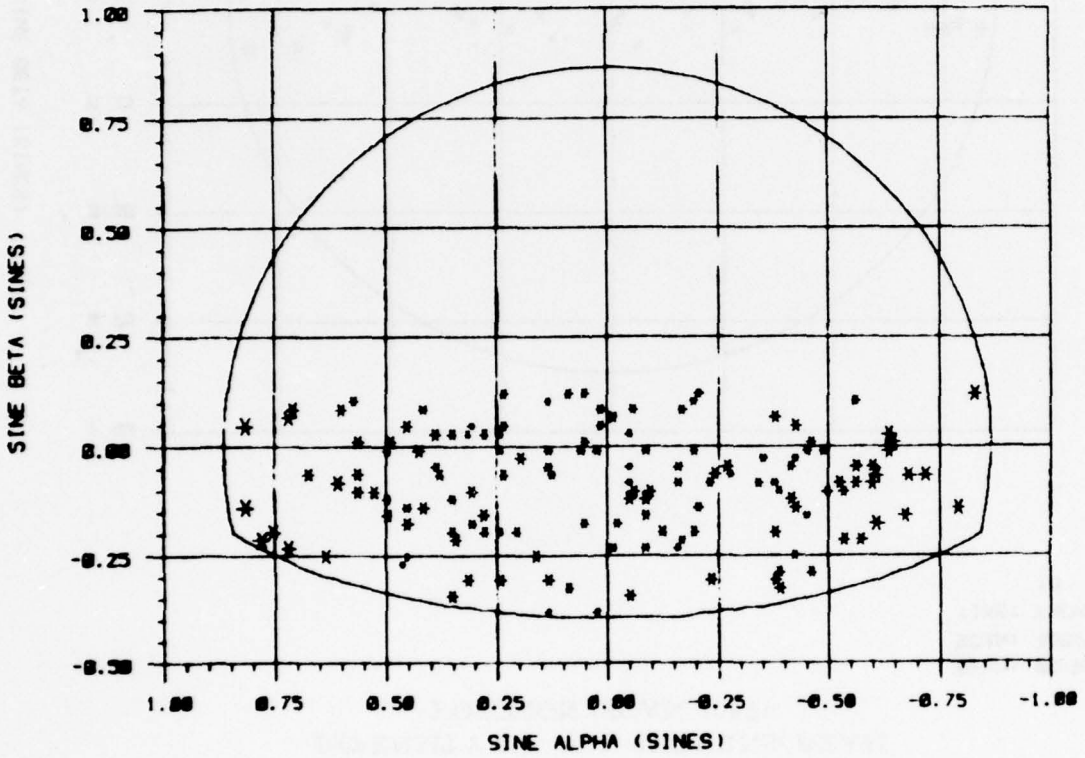

Figure 3-14

SINE SPACE PLOT SHOWING MAXIMUM
INTENSITY OF ALL RETURNS/BEAM
POSITION (SCAN 4059)

BEAM: BOTH
SCAN: 4059
TIME: FROM 86/ 7/ 5/31
TO 86/ 7/ 5/31

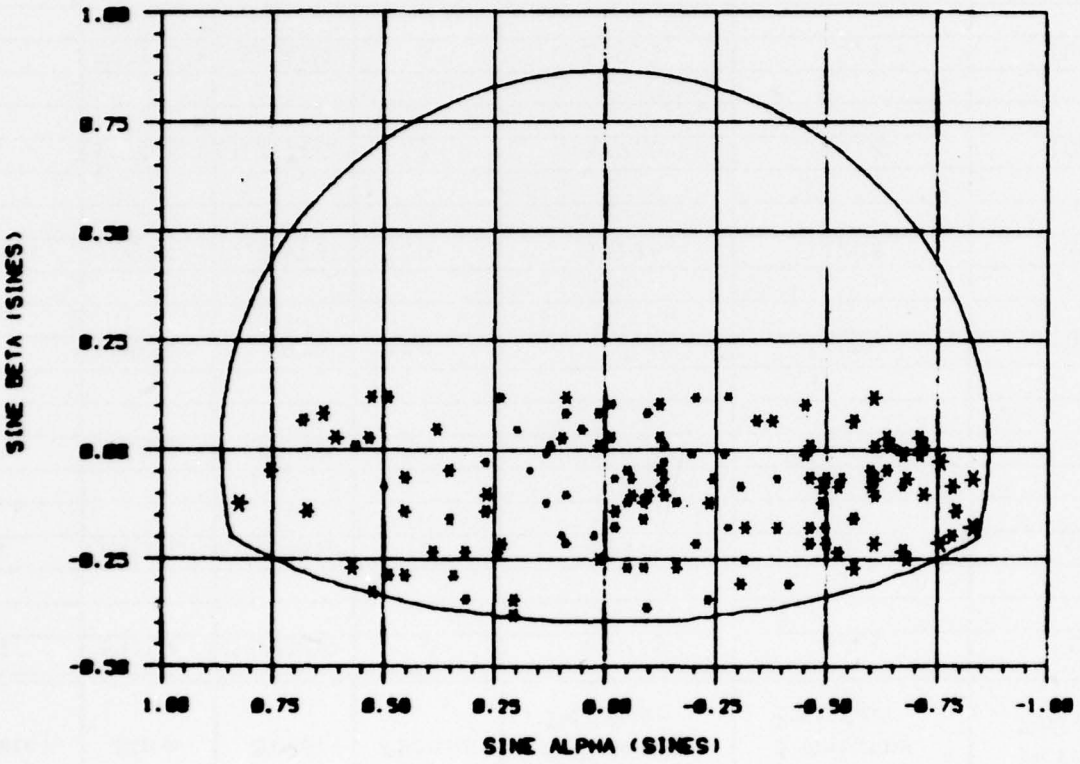

Figure 3-15

AURORA NOISE MEASUREMENTS

Date/Time	*Raster	Sin α	Sin β	#Scans	Mean # Returns Per Scan	Mean # Returns Per Sec	Noise Threshold	Auoral Activity (# Returns)	
								Before	After
92/05/27/08.0**	N	FULL VOLUME		4	417.5	14.6	10dB	34K	44K
92/05/29/00.0									
92/06/19/38.5**	N	FULL VOLUME		12	413.8	14.5	10dB	43K	UNK
92/06/24/50.5									
92/06/27/29.5**	N	FULL VOLUME		21	4830.9	169.5	8dB	UNK	≈40K
92/06/37/50.0									
92/06/40/17.0	S	.0974	-.2679	160	92.9	140.9	8dB	35K	40K
92/06/42/04.0									
92/06/43/24.2	S	.0974	-.2679	160	94.25	142.8	8dB	38K	38K
92/06/45/32.0									
92/07/10/53.0	N	FULL VOLUME		3	377.3	13.2	10dB	54K	54K
92/07/12/17.0									
92/07/28/39.0	N	FULL VOLUME		3	249.3	8.7	10dB	55K	55K
92/07/29/53.0									
92/07/48/37.0	N	FULL VOLUME		3	265.6	9.3	10dB	50K	53K
92/07/49.51.0									
92/08/16/59.0	N	FULL VOLUME		11	228.1	8.0	10dB	50K	56K
92/08/21/41.0									

Table 3-2

AURORA NOISE MEASUREMENTS
(Continued)

Date/Time	Raster	Sin α	Sin β	#Scans	Mean # Returns Per Scan	Mean # Returns Per Sec	Noise Threshold	Auoral Activity (# Returns)	
								Before	After
92/08/30/27.5	N	FULL VOLUME		10	51.1	1.8	10dB	48K	66K
92/08/34/13.0									
92/08/42/41.0	N	FULL VOLUME		3	239.3	8.4	10dB	40K	48K
92/08/44/09.0									
* S = SPSE N = NORMAL AURORA RASTER									
** TRANSMITTERS OFF									

Table 3-2

SINE SPACE PLOT SHOWING MAXIMUM
INTENSITY OF ALL RETURNS/BEAM
POSITION (SCANS 737, 738 AND 739)

TIME: FROM 92/ 8/42/13
TO 92/ 8/43/29

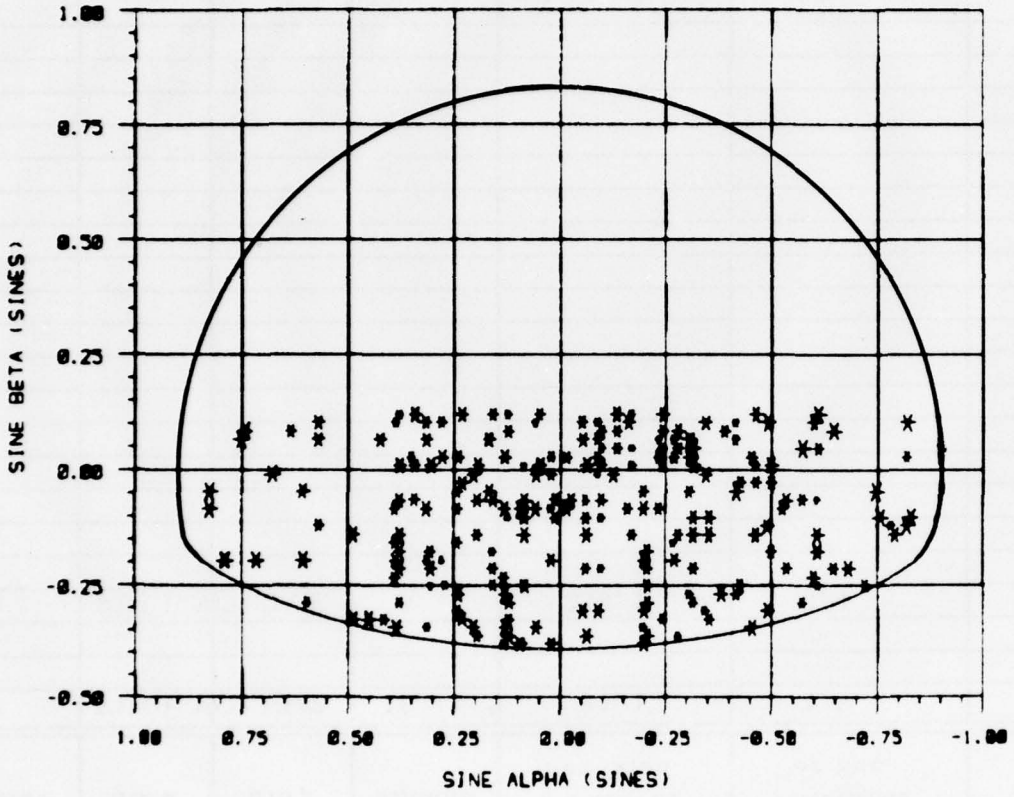

Figure 3-16

Figure 3-17 shows returns from Scan 737 only. Note the concentration of returns at the same coordinates. Figure 3-18 shows returns from Scans 737 and 738. The apparent concentration is almost 20° higher in elevation than radar aurora is expected to occur.

Figures 3-19 through 3-21 show a second sequence of plots in sine space showing the maximum echo intensity at each coordinate. During the construction of the composite (Figure 3-19), and apparent westward motion of returns was noticed. Figures 3-20 and 3-21, when overlaid, show what appears to be the westward flow mentioned above. Due to the nature of noise, it is not unreasonable for random detections to exhibit a trend in a given direction; however, a more normal result would be totally random detections exhibiting little, if any, motion.

3.4 Conclusions From the Noise Study

The results of this study effort are inconclusive. It is evident that there was insufficient data to support a detailed evaluation. It is evident, however, in the limited cases where full sine space scans were available, that the noise does not appear to emanate uniformily from all directions. There were also some video noise peaks of suprisingly high magnitude (40 dB s/n, or better). These may have been bi-static reflections. It can, however, be stated that with a constant noise threshold, the false-alarm rate of the PAR was not significantly changed from its nominal quiescent value, even during the most intense geomagnetic activity and the highest auroral reflectivity.

SINE SPACE PLOT SHOWING MAXIMUM
INTENSITY OF ALL RETURNS/BEAM
POSITION (SCAN 737)

TIME: FROM 92/ 8/42/13
TO 92/ 8/43/29

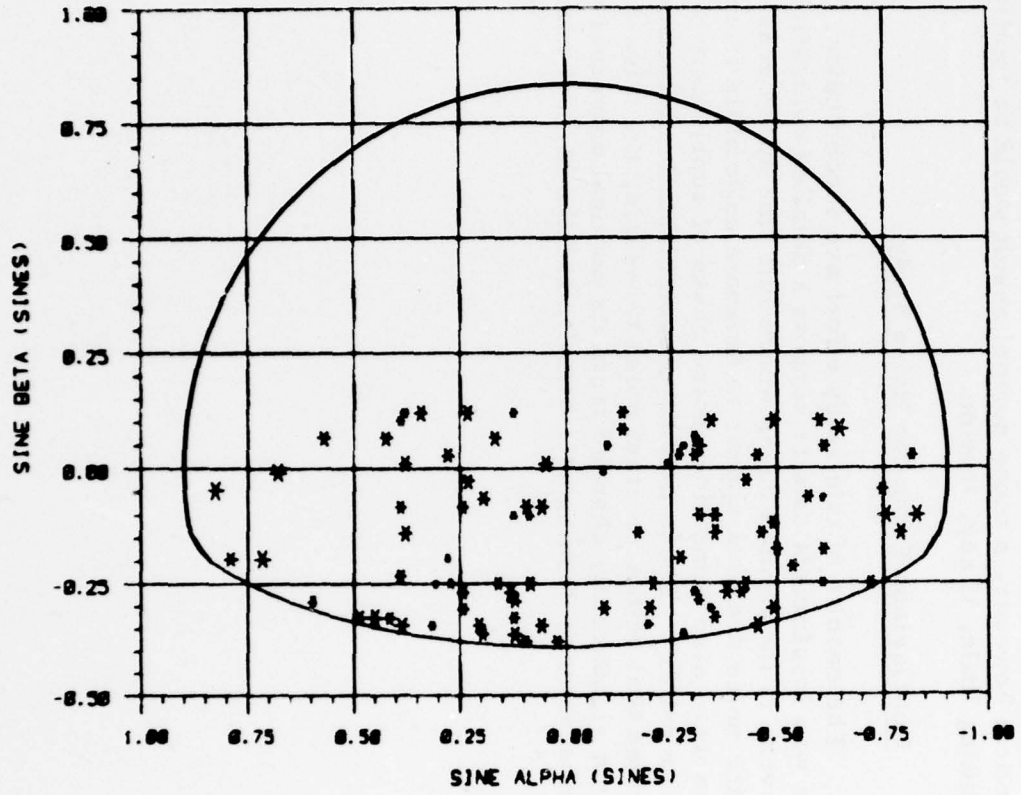

Figure 3-17

SINE SPACE PLOT SHOWING MAXIMUM
INTENSITY OF ALL RETURNS/BEAM
POSITION (SCANS 737 AND 738)

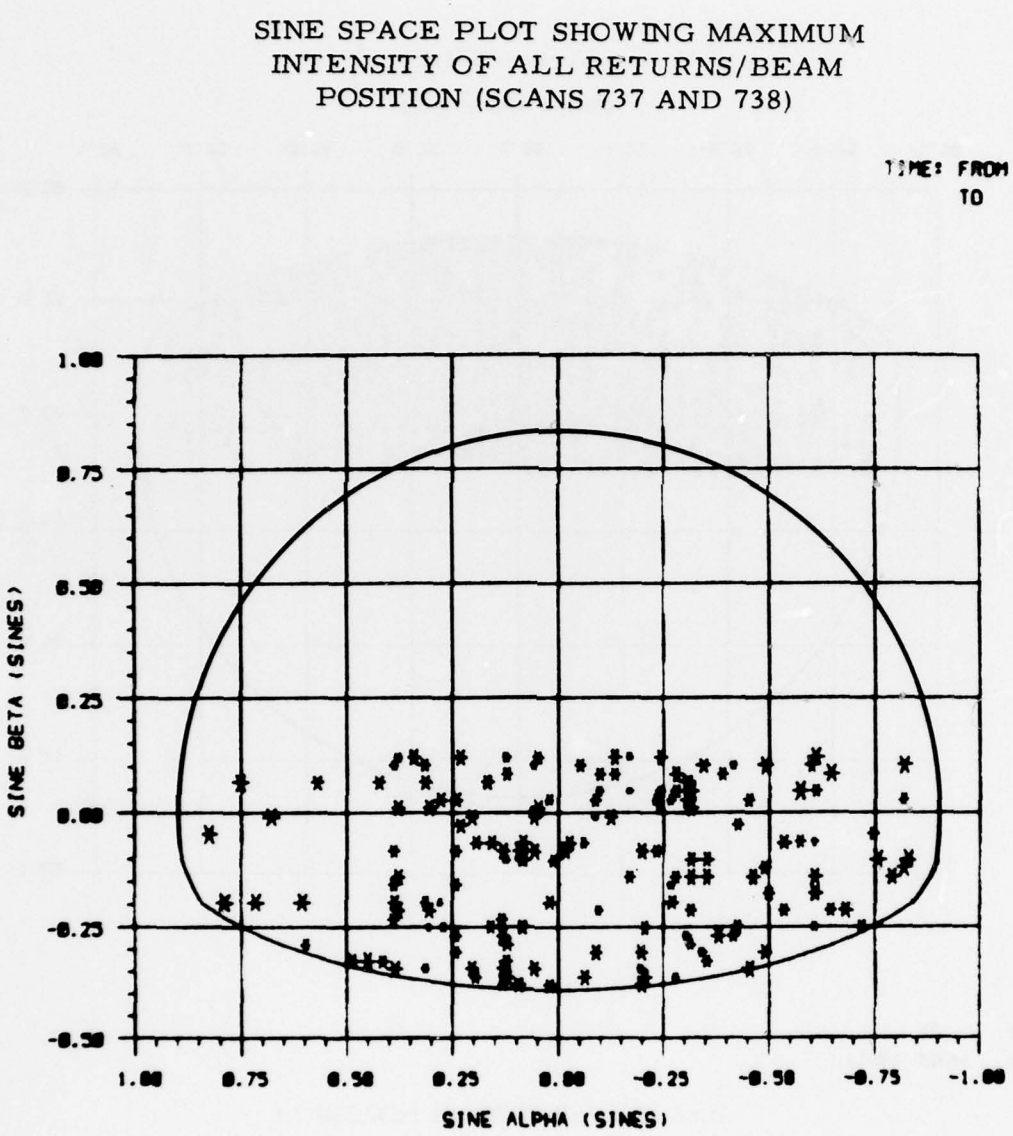

Figure 3-18

SINE SPACE PLOT SHOWING MAXIMUM
INTENSITY OF ALL RETURNS/BEAM
POSITION (SCANS 693 TO 703)

TIME: FROM 92/ 8/16.31
TO 92/ 8/21.31

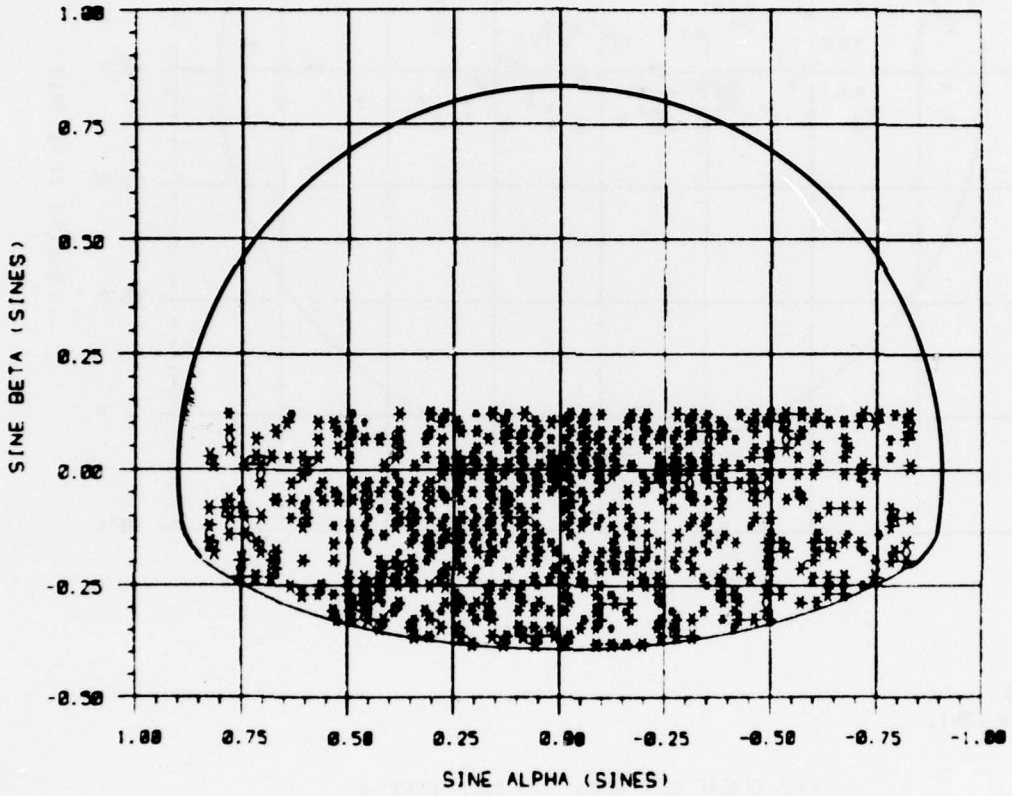

Figure 3-19

SINE SPACE PLOT SHOWING MAXIMUM
INTENSITY OF ALL RETURNS/BEAM
POSITION (SCANS 693 TO 703)

TIME: FROM 92/ 8/16/31
TO 92/ 8/21/31

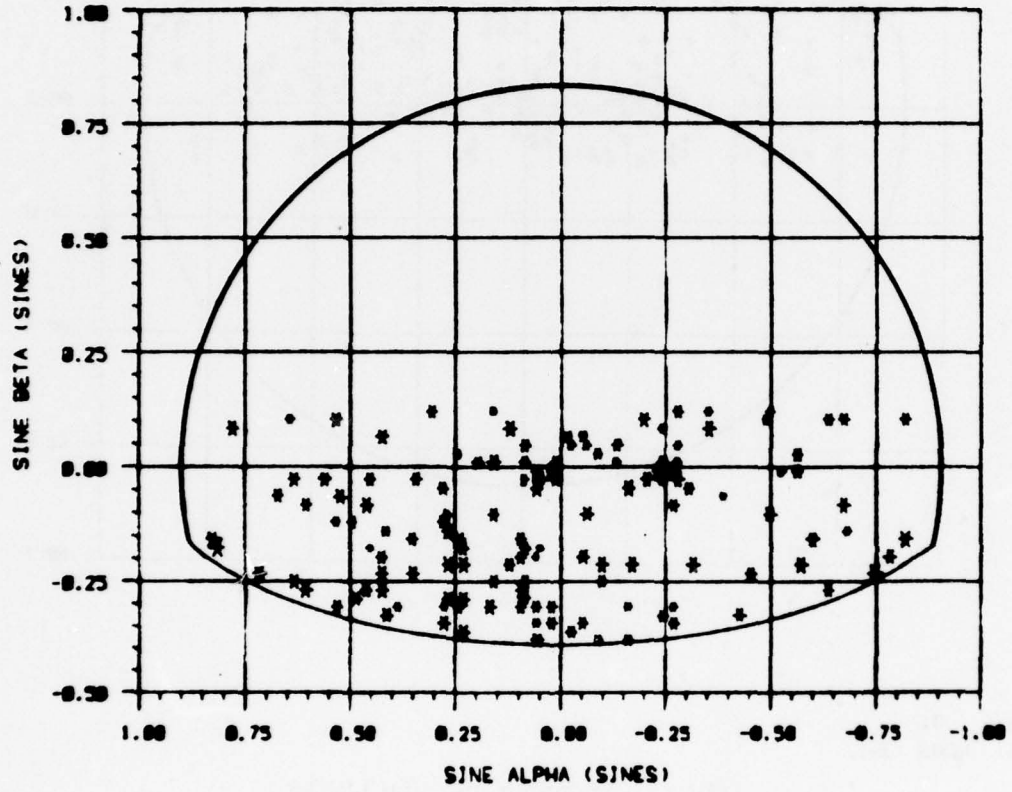

Figure 3-20

SINE SPACE PLOT SHOWING MAXIMUM
INTENSITY OF ALL RETURNS/BEAM
POSITION (SCANS 693 TO 703)

TIME: FROM 92/ 8/16/31
TO 92/ 8/21/31

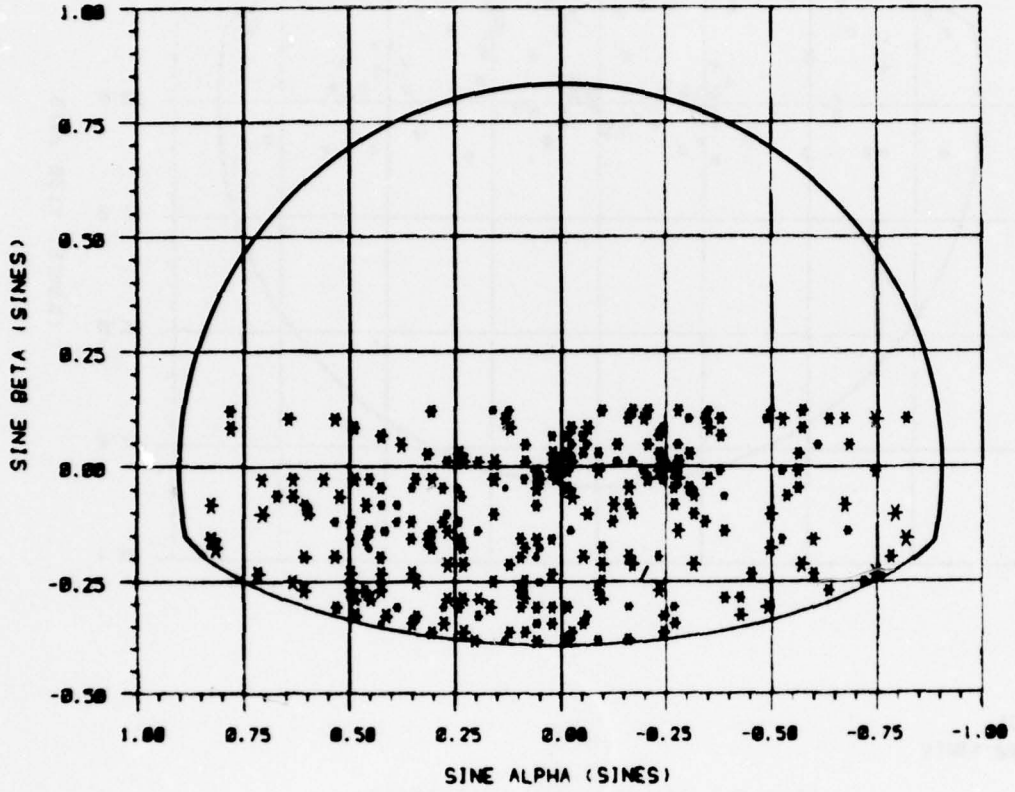

Figure 3-21

4. OVERALL CONCLUSIONS

The sidelobe blanking study has shown that the existing Q-channel provides a reduction of about 10 percent in the number of detected video peaks as compared to the number which would be measured with no sidelobe blanking. However, a significant number of sidelobe echoes are still detected. A large number of these echoes result from vestigial grating lobe peaks which are not blanked by the PAR Q-channel. Most of these echoes will not be eliminated by the radar's auroral exclusion mask. The presence of these unwanted echoes is apparent in much of the processed auroral data. Examination of data collected during periods of high auroral reflectivity suggest that three critical vestigial grating lobes may contribute approximately 26 unwanted detections per second. This represents an additional load on system resources.

REFERENCES

[1] Mitchell, M. J., PAR Auroral Study, Volume I, M&S Computing, Inc., Report No. 76-0013, March 18, 1976.

[2] Mitchell, M. J., PAR Auroral Study, Volume II, M&S Computing, Inc., Report No. 76-0016, May 12, 1976.

[3] Mitchell, M. J., Alley, P. L., Brown, J. L., Cochran, M., PAR Auroral Study, Volume III, M&S Computing, Inc., Report No. 76-0027, August 6, 1976.

[4] Brown, J. L., PAR Auroral Study, Volume III, M&S Computing, Inc., Report No. 76-0042, September 1, 1976.

[5] Brown, J. L., Mitchell, M. J., PAR Auroral Study, Volume V, M&S Computing, Inc., Report No. 76-0052, October 19, 1976.

[6] Howell, J. O., Evaluation of Safeguard Data Processing System Throughput and Error Checking Equipment and Verificiation of Radar Hardware Design, Volume I, M&S Computing, Inc., Report No. 75-0023, July 15, 1975.